

# Removing beam asymmetry bias in precision CMB temperature and polarisation experiments

Christopher G. R. Wallis<sup>1\*</sup>, Michael L. Brown<sup>1</sup>, Richard A. Battye<sup>1</sup>,  
Giampaolo Pisano<sup>1</sup> and Luca Lamagna<sup>2</sup>

<sup>1</sup>*Jodrell Bank Centre for Astrophysics, School of Physics and Astronomy, The University of Manchester, Manchester M13 9PL*

<sup>2</sup>*Dipartimento di Fisica, Sapienza Università di Roma, Piazzale Aldo Moro 5, 00185 Roma, Italy*

Accepted 2014 XXXXX XX. Received 2014 XXXXX XX; in original form 2014 XXXXX XX

## ABSTRACT

Asymmetric beams can create significant bias in estimates of the power spectra from CMB experiments. With the temperature power spectrum many orders of magnitude stronger than the B-mode power spectrum any systematic error that couples the two must be carefully controlled and/or removed. Here, we derive unbiased estimators for the CMB temperature and polarisation power spectra taking into account general beams and general scan strategies. A simple consequence of asymmetric beams is that, even with an ideal scan strategy where every sky pixel is seen at every orientation, there will be residual coupling from temperature power to B-mode power if the orientation of the beam asymmetry is not aligned with the orientation of the co-polarisation. We test our correction algorithm on simulations of two temperature-only experiments and demonstrate that it is unbiased. The simulated experiments use realistic scan strategies, noise levels and highly asymmetric beams. We also develop a map-making algorithm that is capable of removing beam asymmetry bias at the map level. We demonstrate its implementation using simulations and show that it is capable of accurately correcting both temperature and polarisation maps for all of the effects of beam asymmetry including the effects of temperature to polarisation leakage.

**Key words:** methods: data analysis - methods: statistical - cosmology: cosmic microwave back-ground - cosmology: large-scale structure of Universe

## 1 INTRODUCTION

The cosmic microwave background (CMB) has proved to be an incredibly useful tool for testing cosmological models. The CMB two-point correlation functions, or alternatively in Fourier space the power spectra, of the temperature and polarisation fluctuations are of particular interest. There has been a wealth of experiments which have been successful at characterising the CMB power spectra and these observations are consistent with the standard  $\Lambda$ CDM cosmological model (see e.g. Planck Collaboration et al. 2013c). The temperature power spectrum is now extremely well characterised (Planck Collaboration et al. 2013a) and ongoing and future experiments will focus on characterising the polarization more accurately.

The polarisation of the CMB, being a spin-2 field, can be decomposed into curl-free (*E*-mode) and gradient-free (*B*-mode) components. *E*-modes have been successfully detected and characterised, and have helped to constrain cosmology (Kovac et al. 2002; Readhead et al. 2004; Montroy et al. 2006; Brown et al. 2009; Chiang et al. 2010; QUIET Collaboration et al. 2012). The

fainter *B*-mode signal presents a much greater challenge for experimentalists, though the first tentative detections of *B*-mode polarization on small scales are now being made through cross-correlations (Hanson et al. 2013; Polarbear Collaboration et al. 2013).

The *E*-mode power spectrum is approximately two orders of magnitude fainter than the temperature power spectrum while the *B*-mode power spectrum is expected to be at least 2 orders of magnitude fainter still (Challinor 2013). This means that in any experiment aimed at detecting *B*-modes, systematic effects that could potentially couple the temperature or *E*-mode signal to the *B*-mode power spectrum must be strictly controlled. One source of potential error is an asymmetric optical response function (i.e. the experimental beam). During the data analysis for CMB experiments, one often assumes that the beam is axisymmetric so that its effect is to simply (and isotropically) smooth the sky. This assumption can result in a bias in subsequent power spectrum estimates if, as is often the case in reality, the beam is not perfectly axisymmetric.

At present this has not been crucial in extracting CMB power spectra, but with increased sensitivity of instruments, this bias will be important for future experiments. Currently there are three approaches in the literature that attempt to deal with this effect. The

\* E-mail: cwallis@jb.man.ac.uk

first is simply to quantify the systematic error on the cosmological parameters caused by the asymmetry and be satisfied that they are below the statistical uncertainty. This can be done by simulating an experiment's full beam response (Mitra et al. 2011) and propagating the error (Planck Collaboration et al. 2013b). This approach is effective as the error in the maps can be estimated. In their analysis the *Planck* team accounted for the effects of beam asymmetry by finding the most suitable axisymmetric effective beam transfer function to deconvolve the recovered power spectrum. Any further asymmetry bias was shown to have little to no effect on the science (Planck Collaboration et al. 2013a). The second method investigated attempts a full deconvolution of the Time Ordered Data (TOD) from a CMB experiment to remove the effect completely (Wandelt & Górski 2001; Challinor et al. 2000; Keihänen & Reinecke 2012). The results of this method are encouraging but it is not able to deal with certain unavoidable real-world complications. In particular when noise is added to the TOD the deconvolution no longer works for high multipoles. In addition, the deconvolution only works if the experiment observes the entire sky. This is not a significant problem for satellite-based experiments but for ground- or balloon-based experiments this will obviously not be the case.

A third approach is to calculate, and subsequently correct for, the asymmetry bias on the measured pseudo- $C_\ell$  in an experiment (Ramamonjisoa et al. 2013; Souradeep et al. 2006). As presently formulated this is unable to deal with a cut sky without apodising the azimuthal dependence of the mask. This in turn results in a reduction of the cosmological information content of the TOD which is something that we would like to avoid. In addition, these authors assume that each sky pixel is seen in a single orientation only, whereas, in general, experiments will observe each sky pixel in a number of different orientations.

In this paper, we present two methods to remove the effect of asymmetry bias. The first is an algorithm to recover the CMB power spectra using the pseudo- $C_\ell$  approach. We make no assumptions about the beam or the scan strategy in developing unbiased estimators for the underlying CMB temperature and polarisation power spectra. We also show that noise can be easily accommodated. The pseudo- $C_\ell$  estimator that we propose is based on a calculation similar to one presented in Hanson, Lewis, & Challinor (2010). Here, we extend the analysis to polarisation and demonstrate its implementation on simulated temperature-only experiments. Since the estimator works directly on the time ordered data (TOD), it is sub-optimal for polarisation experiments that do not directly measure both  $Q$  and  $U$  Stokes parameters in the timeline (e.g. via detector differencing). For such experiments, the estimator will perform the decomposition into  $Q$  and  $U$  at the level of the power spectrum which will contribute to the statistical error. However, this estimator is well suited to an experiment such as *Planck* which has both instrument- $Q$  and instrument- $U$  detector pairs on its focal plane.

In addition to the pseudo- $C_\ell$  approach, we present a new map-making algorithm that is capable of making temperature and polarisation maps cleaned of asymmetry bias. The map-making algorithm produces maps containing the sky signal smoothed with just the axisymmetric components of the beam and noise. Note that this map-making scheme requires a suitable scan strategy — in general, the more complex the beam asymmetry is, the more redundancy (in terms of polarization angle coverage) is required in the scan strategy. For the asymmetric beams that we have investigated in this paper, the scan strategy requirements are fully met by scanning

modes proposed for future CMB satellite experiments such as those described in Bock et al. (2009).

Removing the asymmetry at the map level has two main benefits. Firstly, in contrast to the case of the pseudo- $C_\ell$  approach, the polarisation power spectrum estimator error bars are not affected by the sample variance of the temperature power spectrum. Secondly, the resulting bias-free temperature and polarisation maps can also be used for science other than power spectrum estimation. Foregrounds can be removed after the map-making has been performed meaning that current component separation techniques can be applied.

The paper is organized as follows. We begin in Section 2 where we present some basic definitions and develop the mathematical formalism on which our algorithms are based. In Section 3, we present the pseudo- $C_\ell$  based approach to correcting for beam asymmetry. Section 4 discusses the potential impact of beam asymmetries on CMB polarization experiments, if they are left uncorrected. In Section 5, we present a technique to correct for the effects of beam asymmetry in the map domain. Section 6 discusses some details of the decomposition of the beam which is required for both of our approaches. We demonstrate our techniques on simulations in Sections 7 & 8 and our conclusions are presented in Section 9.

## 2 BASIC DEFINITIONS AND PRELIMINARIES

Our objective is to construct estimators for the temperature and polarisation fluctuation power spectra given a TOD. We assume that any non-astrophysical signals in the TOD have been flagged and, for the pseudo- $C_\ell$  approach, that foregrounds have been removed and/or masked. We consider an asymmetric beam and a general scan strategy. We begin by defining some relevant quantities.

The CMB temperature and polarisation fluctuations,  $\Delta T(\theta, \phi)$ ,  $Q(\theta, \phi)$  and  $U(\theta, \phi)$ , can be decomposed into spin-weighted spherical harmonics

$$a_{0\ell m} = \int d\Omega {}_0Y_{\ell m}^*(\Omega) \Delta T(\Omega) \quad \text{and} \quad (1)$$

$$a_{\pm 2\ell m} = \int d\Omega {}_{\pm 2}Y_{\ell m}^*(\Omega) [Q(\Omega) \mp iU(\Omega)], \quad (2)$$

where  ${}_sY_{\ell m}$  are the spin weighted spherical harmonics. The temperature,  $E$ -mode and  $B$ -mode harmonic coefficients are related to these by

$$a_{\ell m}^T = a_{0\ell m}, \quad (3)$$

$$a_{\ell m}^E = -\frac{1}{2} (a_{2\ell m} + a_{-2\ell m}), \quad (4)$$

$$a_{\ell m}^B = -\frac{1}{2i} (a_{2\ell m} - a_{-2\ell m}). \quad (5)$$

We are interested in obtaining unbiased estimates for the power and cross spectra of the CMB defined as

$$C_\ell^{XY} = \frac{1}{2\ell + 1} \sum_{m=-\ell}^{\ell} a_{\ell m}^X a_{\ell m}^{Y*}, \quad (6)$$

where  $X, Y = \{T, E, B\}$ .

The response of a telescope to the Stokes parameters on the sky ( $T, Q, U$ ) can be described by some response (beam) functions ( $\tilde{T}, \tilde{Q}, \tilde{U}$ ). The total detected power is

$$W \propto \int (T\tilde{T} + Q\tilde{Q} + U\tilde{U}) d\Omega. \quad (7)$$

For details of how polarised detectors respond to the CMB see

Challinor et al. (2000). One element of the TOD is then this power  $W$  integrated over the time interval between two samples. We define the spin weighted spherical harmonic transforms of the beam to be

$$b_{0\ell k} = \int d\Omega {}_0Y_{\ell k}^*(\Omega) \tilde{T}(\Omega) \quad \text{and} \quad (8)$$

$$b_{\pm 2\ell k} = \int d\Omega {}_{\pm 2}Y_{\ell k}^*(\Omega) [\tilde{Q}(\Omega) \mp i\tilde{U}(\Omega)], \quad (9)$$

when the beam is pointing in the  $z$ -direction in a fiducial orientation such that the co-polarisation is aligned with the  $y$ -direction. Note that this formalism can describe all aspects of a detector's response function. For example, we can include both the asymmetry of the beam and any cross-polarisation response. This will allow us to remove any bias that these beam imperfections would impart on the estimated power spectra.

We truncate our expansion of both the beam and the sky at some maximum multipole,  $\ell_{\max}$ . We also cap the expansion of the beam in  $k$  at some maximum value,  $k_{\max}$ . This is a reasonable approximation to make as beam response functions are typically close to axisymmetric. In Section 6 we will examine this assumption for some specific cases. The beam is then rotated around the sky in a scan to measure the CMB. We describe this rotation using Euler angles  $\omega = [\phi, \theta, \psi]$ . This is really three active rotations. They are active as the beam moves with respect to the coordinate system. The following series of steps describe how to rotate the beam from the fiducial orientation to the orientation described by  $\omega$ , all rotations being performed anticlockwise when looking down the axis by which they are defined.

- (i) The beam is rotated around the  $z$  axis by  $\psi$ .
- (ii) The beam is rotated by  $\theta$  around the  $y$  axis.
- (iii) The beam is rotated around the  $z$  axis again by  $\phi$ .

The Wigner D-matrix,  $D_{mk}^\ell(\omega)$ , performs the required rotations on the spherical harmonic decomposition of a function. Therefore we can write one element of the TOD ( $t_j$ ) as

$$t_j = \sum_{s\ell mk} D_{mk}^{\ell*}(\omega_j) b_{s\ell k}^* a_{s\ell m}. \quad (10)$$

For simplicity, in this paper, we only write the index which is being summed over and not the ranges. For the rest of this paper one should assume  $\ell$  ranges from 0 to  $\ell_{\max}$ ,  $m$  from  $-\ell$  to  $\ell$  and  $s=0, \pm 2$ . The index  $k$  ranges from  $-k_{\max}$  to  $k_{\max}$ , unless  $\ell < k_{\max}$ , in which case the range is the same as for  $m$ .

Before we can go further we must define some more mathematical constructs. The first is the ‘‘hit cube’’,  $W(\omega) \equiv \sum_j \delta(\omega - \omega_j)$ , which describes which sky positions the experiment has observed, and in which orientations.  $W(\omega)$  is defined on the space running from 0 to  $\pi$  in  $\theta$  and from 0 to  $2\pi$  in both  $\phi$  and  $\psi$ . The infinitesimal volume element of this space  $d^3\omega = \sin\theta d\theta d\phi d\psi$ .

The convolution of the sky with the beam  $t(\omega)$  is a continuous function which we only have limited knowledge of. The knowledge we have is dictated by the scan strategy, or in this formalism the hit cube. Formally we have

$$t(\omega) = \sum_{s\ell mk} D_{mk}^{\ell*}(\omega) b_{s\ell k}^* a_{s\ell m}, \quad (11)$$

$$\tilde{t}(\omega) = W(\omega) t(\omega). \quad (12)$$

$\tilde{t}(\omega)$  is a function which contains all of the astrophysical information present in the experiment. It is simply a rewriting of the TOD, where each element is described by a  $\delta$ -function at the relevant orientation  $\omega$ .

The Wigner D-matrices provide a complete orthogonal basis for this space, so we use them to decompose both the TOD and the hit cube as

$$T_{mk}^{\ell*} = \int d^3\omega D_{mk}^\ell(\omega) \tilde{t}(\omega) n(\omega) \quad \text{and} \quad (13)$$

$$w_{mk}^\ell = \frac{2\ell+1}{8\pi^2} \int d^3\omega D_{mk}^{\ell*}(\omega) W(\omega) n(\omega). \quad (14)$$

Here, we have introduced the weighting function  $n(\omega)$ , which ranges from 0 to 1. We use this function to down-weight noisy pixels, apply a foreground mask and/or apodise the hit cube so that it can be described well within our expansion.<sup>1</sup> We use the prefactor in equation (14) to correctly normalise the coefficients so that we can write

$$W(\omega) n(\omega) = \sum_{\ell mk} w_{mk}^\ell D_{mk}^\ell(\omega). \quad (15)$$

For this reconstruction of the hit cube to be exact, one would require  $k$  to range from  $-\ell$  to  $\ell$ , not as we have here from  $-k_{\max}$  to  $k_{\max}$ . This is not a problem for our proposed techniques since, as we shall see later, we only need to capture the features in the  $\psi$  direction with Fourier modes up to some  $k_{\max}$ , the value of which is determined by the complexity of the beam asymmetry. This is analogous to the axisymmetric case, where to recover the temperature fluctuation power spectrum the analysis uses the hit map, which is just the  $k=0$  Fourier mode of the hit cube. So while we cannot fully recover the complete hit cube we do recover its important features.

### 3 BEAM ASYMMETRY CORRECTION WITHIN THE PSEUDO- $C_\ell$ FRAMEWORK

In this section, we develop a technique to correct for the effects of beam asymmetry within the framework of pseudo- $C_\ell$  power spectrum estimators (Hivon et al. 2002; Brown, Castro, & Taylor 2005). As described earlier, this approach to correcting for beam asymmetries is well suited to experiments that can measure the  $Q$  and  $U$  Stokes parameters simultaneously in the timestream (e.g. differencing experiments). In Appendix A we show that for such an experiment the pseudo- $C_\ell$  presented here is similar to that of the standard pseudo- $C_\ell$  approach (Brown, Castro, & Taylor 2005).

#### 3.1 Definition of the pseudo- $C_\ell$ spectra

We wish to define a two-point statistic that contains the relevant information from the TOD and which can also be related to the power spectra defined in equation (6) via a coupling matrix. As the quantity  $T_{mk}^\ell$  contains all of the information present in the TOD, it must therefore contain all of the information required to recover the CMB spectra. We define the pseudo- $C_\ell$  spectra as

$$\tilde{C}_\ell^{kk'} \equiv \sum_m T_{mk}^{\ell*} T_{mk'}, \quad (16)$$

<sup>1</sup> Specifically we consider a weighting function that openly depends on  $\theta$  and  $\phi$ . Our choice of normalised weighting function for a given sky pixel is  $n(p) = m(p)/N_{\text{hits}}(p)$ , where  $m(p)$  is the mask applied to pixel  $p$  and  $N_{\text{hits}}(p)$  is the number of hits that pixel  $p$  receives in the scan strategy. Weighting a TOD element with a factor of  $1/N_{\text{hits}}(p)$  is equivalent to the weight the element receives when making a binned map and should not be considered to be down weighting high signal to noise regions of the map.

which can be computed directly from the TOD. The appropriateness of this choice becomes clear when we write the Wigner D-matrices in terms of the spin weighted spherical harmonics, from equation (3.10) in Goldberg et al. (1967):

$$D_{mk}^\ell(\phi, \theta, \psi) = \sqrt{\frac{4\pi}{2\ell+1}} e^{ik\psi} {}_{-k}Y_{\ell m}(\theta, \phi). \quad (17)$$

We see that  $T_{m0}^\ell$  will be similar to the  $a_{0\ell m}$  coefficients of a binned map made from the TOD while  $T_{m,\pm 2}^\ell$  will be similar to the  $a_{\pm 2\ell m}$  coefficients. This is due to the fact that the Wigner D-matrices are decomposing the 3D space,  $\omega$ , with basis functions over the  $\theta$  and  $\phi$  dimensions which are the spin weighted spherical harmonics.

### 3.2 Calculating the coupling operator

Here we aim to find an analytic expression for the  $\tilde{C}_\ell^{kk'}$  defined in equation (16) in terms of the true sky spectra and a coupling matrix that depends only on the scan strategy and the beam. We begin by re-writing the decomposition of the TOD using equation (10) and the definition of the window function. We do this to replace the sum over  $j$  with an integral,

$$\begin{aligned} T_{m_1 k_1}^{\ell_1*} &= \sum_j D_{m_1 k_1}^{\ell_1}(\omega_j) t_j n(\omega_j) \\ &= \sum_{j s_2 \ell_2 m_2 k_2} D_{m_1 k_1}^{\ell_1}(\omega_j) D_{m_2 k_2}^{\ell_2*}(\omega_j) b_{s_2 \ell_2 k_2}^* a_{s_2 \ell_2 m_2} n(\omega_j). \end{aligned}$$

Using the definition of the hit cube  $W(\omega) = \sum_j \delta(\omega - \omega_j)$  we deduce that

$$T_{m_1 k_1}^{\ell_1*} = \sum_{s_2 \ell_2 m_2 k_2} b_{s_2 \ell_2 k_2}^* a_{s_2 \ell_2 m_2} K_{m_1 k_1 m_2 k_2}^{\ell_1 \ell_2}, \quad (18)$$

where in the last line we have introduced the coupling kernel,

$$K_{m_1 k_1 m_2 k_2}^{\ell_1 \ell_2} \equiv \int d^3\omega D_{m_1 k_1}^{\ell_1}(\omega) D_{m_2 k_2}^{\ell_2*}(\omega) W(\omega) n(\omega). \quad (19)$$

We are now in a position to calculate the coupling operator. We start from the definition of  $\tilde{C}_\ell^{k_1 k'_1}$ ,

$$\begin{aligned} \tilde{C}_{\ell_1}^{k_1 k'_1} &\equiv \sum_{m_1} T_{m_1 k_1}^{\ell_1*} T_{m_1 k'_1}^{\ell_1} \\ &= \sum_{\substack{m_1 \\ s_2 \ell_2 m_2 k_2 \\ s_3 \ell_3 m_3 k_3}} b_{s_2 \ell_2 k_2}^* a_{s_2 \ell_2 m_2} K_{m_1 k_1 m_2 k_2}^{\ell_1 \ell_2} \\ &\quad \times b_{s_3 \ell_3 k_3} a_{s_3 \ell_3 m_3}^* K_{m_1 k'_1 m_3 k_3}^{\ell_1 \ell_3*}. \end{aligned} \quad (20)$$

If we now assume that the CMB temperature and polarization fluctuations are Gaussian distributed with isotropic variance, then we can write  $\langle a_{s\ell m} a_{s'\ell' m'}^* \rangle = C_\ell^{ss'} \delta_{\ell\ell'} \delta_{mm'}$  where we have defined

$$C_\ell^{ss'} = \frac{1}{2\ell+1} \sum_m a_{s\ell m} a_{s'\ell m}^*. \quad (21)$$

Using this result, equation (20) simplifies to

$$\begin{aligned} \langle \tilde{C}_{\ell_1}^{k_1 k'_1} \rangle &= \sum_{\substack{m_1 \\ s_2 \ell_2 m_2 k_2 \\ s_3 \ell_3 m_3 k_3}} b_{s_2 \ell_2 k_2}^* K_{m_1 k'_1 m_2 k_2}^{\ell_1 \ell_2} b_{s_3 \ell_3 k_3} K_{m_1 k_1 m_3 k_3}^{\ell_1 \ell_3*} C_{\ell_2}^{s_2 s_3} \\ &= \sum_{\substack{s_2 \ell_2 m_2 k_2 \\ s_3 \ell_3 m_3 k_3}} b_{s_2 \ell_2 k_2}^* b_{s_3 \ell_3 k_3} M_{k_1 k'_1 k_2 k_3}^{\ell_1 \ell_2} C_{\ell_2}^{s_2 s_3}, \end{aligned} \quad (22)$$

where, in the second step, we have used the product of two coupling kernels,  $M_{k_1 k'_1 k_2 k_3}^{\ell_1 \ell_2}$ , derived in Appendix B. We can now identify

the coupling operator that describes the contribution of each sky spectrum  $C_\ell^{s_1 s_2}$  to each of the  $\tilde{C}_\ell^{kk'}$ , i.e. we can write

$$\langle \tilde{C}_{\ell_1}^{k_1 k'_1} \rangle = \sum_{\ell_2 s_2 s_3} O_{\ell_1 \ell_2}^{k_1 k'_1 s_1 s_2} C_{\ell_2}^{s_2 s_3}, \quad (23)$$

where,

$$O_{\ell_1 \ell_2}^{k_1 k'_1 s_1 s_2} = \sum_{k_2 k_3} b_{s_2 \ell_2 k_2}^* b_{s_3 \ell_2 k_3} M_{k_1 k'_1 k_2 k_3}^{\ell_1 \ell_2}. \quad (24)$$

Certain symmetries can be used to reduce the number of  $M$  matrices required to evaluate equation (24). These symmetries, which are derived in Appendix C, are

$$M_{k_1 k'_1 k_2 k_3}^{\ell_1 \ell_2} = M_{k'_1 k_1 k_3 k_2}^{\ell_1 \ell_2*}, \quad (25)$$

$$M_{k_1 k'_1 k_2 k_3}^{\ell_1 \ell_2} = (-1)^{k_2 - k_1 + k_3 - k'_1} M_{-k_1 - k'_1 - k_2 - k_3}^{\ell_1 \ell_2*}. \quad (26)$$

### 3.3 Recovering the true CMB spectra

We are now in a position to obtain unbiased estimators for the true CMB power spectra  $C_\ell^{XY}$  defined in equation (6). We start by defining a large vector made up of the pseudo- $C_\ell$  spectra,  $\tilde{C}_\ell^{kk'}$ , and another comprised of the true full-sky spin spectra,  $C_\ell^{ss'}$  defined in equation (21):

$$\mathbf{C}_i = (C_\ell^{00}, C_\ell^{02}, C_\ell^{0-2}, C_\ell^{22}, C_\ell^{2-2}, C_\ell^{-2-2})^T \quad (27)$$

$$\tilde{\mathbf{C}}_i = (\tilde{C}_\ell^{00}, \tilde{C}_\ell^{02}, \tilde{C}_\ell^{0-2}, \tilde{C}_\ell^{22}, \tilde{C}_\ell^{2-2}, \tilde{C}_\ell^{-2-2})^T. \quad (28)$$

Each of these are vectors of length  $6(\ell_{\max} + 1)$ . Using these definitions we can write our overall coupling matrix equation as

$$\tilde{\mathbf{C}}_{i_1} = \sum_{i_2} \mathbf{O}_{i_1 i_2} \mathbf{C}_{i_2}. \quad (29)$$

We write the overall coupling operator  $\mathbf{O}_{i_1 i_2}$  explicitly in terms of the individual  $O$ -matrices of equation (24) in Appendix D. Once this operator has been calculated, equation (29) can be inverted to recover the true spin spectra  $C_\ell^{ss'}$ , properly deconvolved for both the mask and the asymmetric beam. A further simple transformation, which is explicitly written down in Appendix E, yields the final estimates of the six possible CMB power spectra,  $C_\ell^{XY}$ . Note that, as with normal pseudo- $C_\ell$  estimators, in the presence of a severe sky cut, the matrix,  $\mathbf{O}_{i_1 i_2}$  will be singular and must therefore be binned before it can be inverted. This is standard practice with pseudo- $C_\ell$  power spectrum estimators (Hivon et al. 2002; Brown, Castro, & Taylor 2005).

### 3.4 Including noise

Any useful algorithm for removing the effects of beam asymmetry must also be able to deal with instrumental noise. Since our algorithm works within the framework of the standard pseudo- $C_\ell$  technique, we can use exactly the same approach to remove the noise bias as is adopted in the standard analysis (Hivon et al. 2002). A TOD element including noise can be written as

$$t_j = \sum_{s\ell m k} D_{mk}^\ell(\omega_j) b_{s\ell m}^* a_{s\ell m} + n_j. \quad (30)$$

If we assume that the noise is not correlated with the pointing direction of the telescope then

$$(\tilde{C}_\ell^{kk'})^{\text{SN}} = (\tilde{C}_\ell^{kk'})^{\text{S}} + N_\ell^{kk'}, \quad (31)$$



where the SN and S superscripts denote the signal-plus-noise and the signal-only pseudo- $C_\ell$  spectra respectively. An unbiased estimate of the noise power spectra,  $N_\ell^{kk'}$ , can be obtained by performing a set of simulations containing only instrument noise and calculating  $\tilde{C}_\ell^{kk'}$  for each as before using equation (16). The noise bias is then estimated as the average over the set of noise realisations,  $N_\ell^{kk'} = \langle C_\ell^{kk'} \rangle$ . The final estimator for the full-sky, noise-debiased and asymmetry-cleaned spin power spectra can then be written as

$$\mathbf{C}_{i_1} = \sum_{i_2} \mathbf{O}_{i_1 i_2}^{-1} (\tilde{\mathbf{C}}_{i_2} - \langle \mathbf{N}_{i_2} \rangle), \quad (32)$$

where  $\langle \mathbf{N}_{i_2} \rangle$  is a vector of length  $6(\ell_{\max} + 1)$  comprised of all of the individual noise bias spectra, constructed in an analogous fashion to equations (27) and (28). As before, the six CMB power spectra are then recovered trivially using the relation in Appendix E.

#### 4 IMPACT OF BEAM ASYMMETRIES ON CMB POLARIZATION EXPERIMENTS

With the analysis of the previous two sections in place, we can now examine the effect that beam asymmetries will have on the  $E$ - and  $B$ -mode polarization power spectra. We begin by noting again that the  $T_{m\pm 2}^\ell$  of equation (13) are closely related to the spin-2 harmonic coefficients  $a_{\pm 2\ell m}$  of  $Q$  and  $U$  maps constructed from the same TOD. In analogy with equations (4) and (5), we can therefore define the following  $E$ -mode-like and  $B$ -mode-like linear combinations and two-point correlations of the  $T_{m\pm 2}^\ell$ :

$$T_{mE}^\ell \equiv -\frac{1}{2} (T_{m2}^\ell + T_{m-2}^\ell) \quad (33)$$

$$T_{mB}^\ell \equiv -\frac{1}{2i} (T_{m2}^\ell - T_{m-2}^\ell) \quad \text{and} \quad (34)$$

$$\Rightarrow \tilde{C}_\ell^{EE} = \frac{1}{4} (\tilde{C}_\ell^{22} + \tilde{C}_\ell^{-2-2} + \tilde{C}_\ell^{-22} + \tilde{C}_\ell^{2-2}) \quad (35)$$

$$\Rightarrow \tilde{C}_\ell^{BB} = -\frac{1}{4} (\tilde{C}_\ell^{22} + \tilde{C}_\ell^{-2-2} - \tilde{C}_\ell^{-22} - \tilde{C}_\ell^{2-2}) \quad (36)$$

In Appendix A, we show that the quantities defined in equations (33) and (34) are similar to the standard pseudo- $C_\ell$   $E$ - and  $B$ -modes defined in Brown, Castro, & Taylor (2005). These relations can then be used to investigate the impact of beam asymmetries and/or a non-zero cross-polar beam response function.

Of particular concern is the potential coupling between the temperature power spectrum and the  $B$ -mode polarization power spectrum. As the temperature power spectrum is known to be at least four orders of magnitude stronger than the  $B$ -mode power, any coupling between the two could be catastrophic if not properly accounted for. Here we show how the most prominent asymmetric modes of the beam can potentially create such a coupling.

As described in Section 6 (see Figs. 1 and 2), the  $k = \pm 2$  mode is by far the most prominent asymmetric term for the representative beams that we consider later in this paper. To examine the impact of the  $k = \pm 2$  asymmetry, we consider a situation where all possible orientations are observed, i.e. where  $W(\omega)n(\omega)=1$ , for the normalisation described in section 2. In this case, the contribution to  $T_{m\pm 2}^{\ell*}$  from the temperature fluctuations is

$$\begin{aligned} T_{m\pm 2}^{\ell*} &= \sum_{\ell'm'k'} b_{0\ell'k'}^* a_{0\ell'm'} \int d^3\omega D_{m\pm 2}^\ell(\omega) D_{m'k'}^{\ell'*}(\omega) \\ &= \frac{8\pi^2}{2\ell+1} b_{0\ell\pm 2}^* a_{0\ell m}, \end{aligned} \quad (37)$$

where we have used the orthogonality of the Wigner D-matrices (Goldberg et al. 1967). Equation (37) shows that the asymmetry will couple temperature to polarization even in the case of an ideal scan strategy. This was to be expected, since both the CMB polarisation field and the convolution of the temperature fluctuations with the  $k = \pm 2$  term of the beam are spin- $\pm 2$  quantities. From equations (33) and (34), the effect on the measured the  $E$ - and  $B$ -mode polarisation is

$$\Delta T_{mE}^\ell = -\frac{4\pi^2}{2\ell+1} (b_{0\ell 2} + b_{0\ell -2}) a_{0\ell m}^* \quad \text{and} \quad (38)$$

$$\Delta T_{mB}^\ell = -\frac{4\pi^2}{i(2\ell+1)} (b_{0\ell 2} - b_{0\ell -2}) a_{0\ell m}^*. \quad (39)$$

For the coupling from temperature to  $B$ -mode polarisation to be non-zero in this case, then  $b_{0\ell\pm 2}$  must be complex. This will only be the case if the beam asymmetry is orientated at an angle to the polarisation sensitivity direction defined by the co-polar response, which will not be the case in general.

This result was first found by ?, where they examined statistically varying systematic errors. A statistically varying differential beam ellipticity between a detector pair would couple temperature to polarisation just as our constant ellipticity has. O'Dea, Challinor, & Johnson (2007) also studied the systematic errors induced when an elliptical Gaussian beam is used in a  $B$ -mode experiment. They considered a specific type of ellipticity: one where the beam is either perturbed along the direction of the polarisation, or perpendicular to it. This type of perturbation has the unique property of having a decomposition where  $b_{0\ell\pm 2}$  is real, and therefore such an asymmetry cannot couple temperature fluctuations to  $B$ -mode fluctuations. As O'Dea, Challinor, & Johnson (2007) shows, if the beam is perturbed in any other way than this special case, then temperature fluctuations will be coupled to  $B$ -mode fluctuations even in the case of an ideal scan strategy. This result is in agreement with the findings of Shimon et al. (2008) who also considered the coupling between temperature and  $B$ -mode polarisation due to beam asymmetry effects.

#### 5 BEAM ASYMMETRY CORRECTION DURING MAP-MAKING

In some cases, the approach to correcting for beam asymmetry presented in Section 3 will be sub-optimal. For example, in the case where one corrects for significant temperature-to-polarization leakage, there will be a contribution to the error-bars on the reconstructed polarization power spectra due to the sample variance associated with the leaked temperature signal. In addition, for polarization experiments that do not measure  $Q$  and  $U$  simultaneously in the time-stream, the  $B$ -mode power spectrum errors will be affected by the sample variance associated with the much larger  $E$ -mode polarisation. A technique that corrects for beam asymmetry at the map level will be immune to these issues and is therefore an attractive prospect. Here, we develop such a method to correct for beam asymmetry effects during the map-making step.

We begin by recalling that the convolution of the sky signal with a general beam is given by equation (11). In an experiment a telescope will scan the sky, giving us a set of measurements of this function  $t(\omega)$ . For each pixel on the sky we therefore have a set of measurements at various orientations.

### 5.1 Extracting the temperature and polarisation of a pixel

This discussion is concerned with estimating the temperature and polarisation signal at the position of a single sky pixel. The detected signal at the position of a pixel  $S$  will depend on the instrument orientation at the time of observation  $\psi$  due to the polarisation of the sky and the beam asymmetry. If the beam was axisymmetric and had no polarised response then  $S(\psi)$  would be constant and equal to the beam-smoothed CMB temperature at the pixel location.<sup>2</sup> This can be seen from equation (11) by setting  $b_{s\ell k} = b_{0\ell 0} \delta_{k0} \delta_{s0}$  and noticing that the  $\psi$  dependence of  $t(\omega)$  comes from the Wigner D matrices. For a polarised detector  $S(\psi)$  would then contain  $k=\pm 2$  Fourier modes, due to the spin-2 nature of polarisation. This property is exploited by map-making algorithms to find the temperature and polarisation of a pixel. In these algorithms the  $\psi$  dependence of the detected signal is assumed to be due to the polarisation signal. Here, we relax this assumption and develop a map-making algorithm that provides estimates of the temperature and polarisation of a pixel that are free of systematics of different spins.

We represent the orientations at which a pixel is seen in an experiment by defining a window function  $h(\psi) \equiv \frac{1}{n_{\text{hits}}} \sum_j \delta(\psi - \psi_j)$ , where  $n_{\text{hits}}$  is the number of hits on the pixel.  $h(\psi)$  will be different for each pixel and will be dependant on the scan strategy. The detected signal  $S^d(\psi)$  is therefore

$$S^d(\psi) = h(\psi)S(\psi). \quad (40)$$

In Fourier space<sup>3</sup> this multiplication takes the form of a convolution

$$\tilde{S}_k^d = \sum_{k'=-\infty}^{\infty} H_{kk'} \tilde{S}_{k'}, \quad (41)$$

where we have defined  $H_{kk'} \equiv \tilde{h}_{k-k'}$ . Therefore, if we can invert the matrix  $H_{kk'}$  then we can recover the true  $\tilde{S}_k$ . Recovering the spin-0 and spin-2 features of  $S(\psi)$  is the main goal of this work since these are the CMB temperature and polarisation of the pixel. Therefore, we would like to obtain estimates for  $\tilde{S}_0$  and  $\tilde{S}_{\pm 2}$ .

Inverting the matrix  $H_{kk'}$  as it is written in equation (41) would be impossible: firstly it is infinitely large, and secondly for any realistic  $h(\psi)$  the matrix will be singular.<sup>4</sup> However, if we make the assumption that  $\tilde{S}_k$  cuts off at a small value of  $k_{\text{max}}$  and if the  $\psi$  angle coverage of that pixel is sufficient such that this reduced matrix is invertible then we can use the approximation,

$$\tilde{S}_k = \sum_{k'=-k_{\text{max}}}^{k_{\text{max}}} H_{kk'}^{-1} \tilde{S}_{k'}^d. \quad (42)$$

We can choose  $k_{\text{max}}$  by measuring the azimuthal dependence of the beam and ensuring that we include enough  $k$ -modes to capture all of the Fourier modes in  $S(\psi)$ . As in the case of the pseudo- $C_\ell$  approach (Section 3), the  $k_{\text{max}}$  should be chosen so that the asymmetry of the beam is fully captured. We return to this issue in the following section where we examine the harmonic decomposition of some representative asymmetric beams.

Adopting the HEALPIX<sup>5</sup> definition of the Stokes parameters, we

can calculate the temperature and polarisation of the pixel from the inverse Fourier transform of the estimated  $\tilde{S}_k$  as

$$T = \tilde{S}_0, \quad (43)$$

$$Q = 2\Re(\tilde{S}_2), \quad (44)$$

$$U = 2\Im(\tilde{S}_2). \quad (45)$$

Performing this procedure for all observed pixels, we will then have estimates of the  $T$ ,  $Q$  and  $U$  maps which are free of systematics that have a different spin to our desired quantity. Note we will have not removed systematics that have the same spin. Specifically the coupling from temperature to polarisation due to the asymmetry in the beam discussed in Section 4 will still contaminate our estimates of  $Q$  and  $U$ . We will consider this problem in the following subsection. As we show in the simulation tests in Section 8 there will be a noise penalty associated with this effective re-weighting of the data. For this reason  $k_{\text{max}}$  should be as large as it needs to be to capture all the asymmetry in the beam but no larger as this will increase the noise in the map.

This method is similar to the re-weighting of the data to remove systematics of different spin presented in Bock et al. (2009). Note however that in Bock et al. (2009) study suggests discarding (or down weighting) all data that does not have a "counterpart" that could be used to average systematics to zero. For example, a spin-1 systematic can be removed if every TOD element has a counterpart where the pixel was hit with  $\psi$  orientation  $\pi$  away from the first. Conversely, the method we propose in this paper can use all of the data to characterise the spin-1 systematic and remove it.

### 5.2 Removing the leakage from temperature to polarisation

We showed in Section 4 that the asymmetry of the beam will leak temperature fluctuations to polarisation regardless of the scan strategy. This is due to the spin-2 dependence of the temperature of the CMB convolved with the  $k=\pm 2$  mode of the beam response function. The polarisation maps made using the map-making method described above will still contain this spin-2 leakage from temperature to polarisation. However, since we know that this leakage is from the temperature fluctuations coupling to the  $k=\pm 2$  asymmetry in the beam, and since we also now have an unbiased estimate of the temperature map, we can therefore calculate and remove this leakage.

We start from the estimated temperature map. If we have observed only part of the sky it is necessary to apodise the map such that there are no features due to the mask that are smaller than the beam scale. We then take the spherical harmonic transform of this map,

$$\tilde{a}_{0\ell m} = \int d\Omega_0 Y_{\ell m}^*(\Omega) \tilde{T}(\Omega). \quad (46)$$

We can now calculate the polarization leakage using equations (38) and (39). One can show that the spherical harmonic transform of the temperature leakage is given by

$$\Delta a_{\ell m}^E = 2\Re\left(\frac{b_{0\ell 2}}{b_{0\ell 0}}\right) \tilde{a}_{0\ell m}, \quad (47)$$

$$\Delta a_{\ell m}^B = 2i\Im\left(\frac{b_{0\ell 2}}{b_{0\ell 0}}\right) \tilde{a}_{0\ell m}. \quad (48)$$

Upon transforming back to real space, these terms can then be removed from the polarisation maps. Note that the regions within a beam-scale of the locations where the temperature map was

<sup>2</sup> The detected signal for a pixel  $i$  is related to our previous notation by  $S_i(\psi) = t(\psi, \theta=\theta_i, \phi=\phi_i)$

<sup>3</sup> We define the Fourier transform of  $f(\psi)$  and the inverse transform to be  $\tilde{f}_k = \frac{1}{2\pi} \int_0^{2\pi} d\psi e^{-ik\psi} f(\psi)$  and  $f(\psi) = \sum_{k=-\infty}^{\infty} e^{ik\psi} \tilde{f}_k$ .

<sup>4</sup> Note that "realistic" in this context explicitly excludes the case of an ideal scan strategy for which  $h(\psi)=1$ .

<sup>5</sup> See <http://healpix.sourceforge.net>

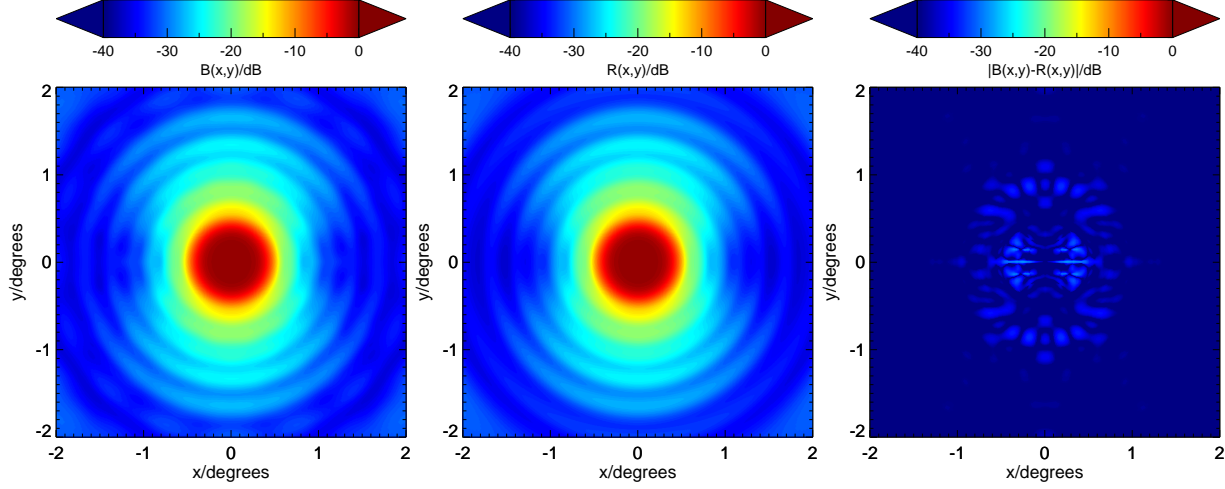


**Figure 1.** *Left panel:* The simulated beam of a 17 moded horn planned to be on board the LSPE balloon experiment. *Centre panel:* the reconstruction of the beam retaining only modes with  $k=0, \pm 2$ . *Right panel:* The absolute error between the simulated beam and the reconstruction.

apositioned should be disregarded as the leakage will not have been removed in these regions.

## 6 EVALUATING THE PARAMETER $k_{\text{max}}$ FOR A TEMPERATURE ONLY EXPERIMENT

Both the pseudo- $C_\ell$  technique and the map-making approach for removing beam asymmetries require us to impose a cap on the harmonic expansion of the beam,  $k_{\text{max}}$ . We now look at a realistic set up for a CMB experiment in order to ascertain how large the required  $k_{\text{max}}$  is likely to be for real experiments. We make no assumption on the scan strategy. However, beam shapes are generally designed to be as axisymmetric as possible. We expect therefore that the beam expansion can be truncated after only a few terms with minimal loss of accuracy. We note that the pseudo- $C_\ell$  correction technique can in principle be applied for any  $k_{\text{max}}$  that is deemed necessary in order to achieve the required accuracy. This will come with the obvious computational cost of increasing the number of summations required to evaluate equation (24). In contrast, for the map-making approach, there will be some maximum value of  $k_{\text{max}}$  for which the matrix  $H_{kk'}$  of equation (42) will be invertible. We also note that increasing  $k_{\text{max}}$  will increase the statistical error on the recovered map. It should therefore be chosen to be only as large as is required by the asymmetry in the beam. In practice, whether the map-making approach will be appropriate for any given experiment will depend on both the complexity of the beam asymmetry and on the polarization angle coverage of the experiment.

### 6.1 Beam decompositions for some representative cases

As a demonstration of how a realistic and asymmetric beam can be represented using just a few  $k$ -modes, we consider a numerical simulation of an instrumental beam corresponding to the multi-moded 145 GHz feed horns planned to be flown on-board the balloon-borne Large Scale Polarisation Explorer (LSPE, The LSPE collaboration et al. 2012). By coupling 17 wave-guide modes, the sensitivity of a single LSPE horn + detector module is greatly increased. However, the large number of propagated modes

results in a complicated and potentially asymmetric overall beam shape. Note that the numerical simulation used here is of the horn only and a simple scaling of the overall beam size has been applied to roughly approximate the effect of the telescope lens.

We note that the LSPE experiment will also include a half-wave plate (HWP) in front of the optics which will be used to increase the polarization angle coverage of the experiment. However, for the purposes of this demonstration, we consider a temperature-only experiment and we therefore ignore the effect of the HWP.

Upon performing the spin-0 decomposition of the beam, (equation 8), we find that only a few azimuthal modes are required to accurately model what might be considered a rather asymmetric beam. Fig. 1 shows the original simulated beam alongside a representation of it retaining only the two most significant modes ( $k = 0$  and  $k = \pm 2$ ) of the decomposition. The major features of the beam asymmetry are clearly well captured using this heavily truncated expansion. We therefore choose to set  $k_{\text{max}}=2$ . The beams shown here are invariant when rotated by  $\pi$ , therefore the odd azimuthal terms will be zero. Explicitly the truncated decomposition of the beam can be written as (now writing  $b_{0lk} = b_{lk}$  etc. for clarity)

$$b_{lk} = b_{l0}\delta_{k0} + b_{l+2}\delta_{k,+2} + b_{l-2}\delta_{k,-2}. \quad (49)$$

In Fig. 1 we also show the residuals between the full beam and this representation which is seen to be a good approximation. We can immediately see from equation (22) that this will greatly simplify the pseudo- $C_\ell$  coupling matrix calculation by limiting the sum over  $k_2$  and  $k_3$  to only include the  $k_2, k_3=0, \pm 2$  modes.

We also examine a general elliptical Gaussian beam described by

$$B(\theta, \phi) = \frac{1}{2\pi q \sigma^2} e^{-\frac{\theta^2}{2\sigma^2} (\cos^2 \phi + q^{-1} \sin^2 \phi)}, \quad (50)$$

where  $q$  is a parameter that defines the asymmetry of the beam and the full width at half maximum (FWHM)  $\theta_{\text{FWHM}} = 2.35\sigma$ . If  $q=1$  then the beam is axisymmetric. To test the expansion we choose  $\theta_{\text{FWHM}}=7$  arcmin and  $q=1.5$ , which represents a highly elliptical beam, significantly more elliptical than one might expect in a real CMB experiment. This simulated beam therefore provides a stringent test of our correction algorithms. We plot the spin-0 decomposition of this beam in Fig. 2. It is encouraging to see that

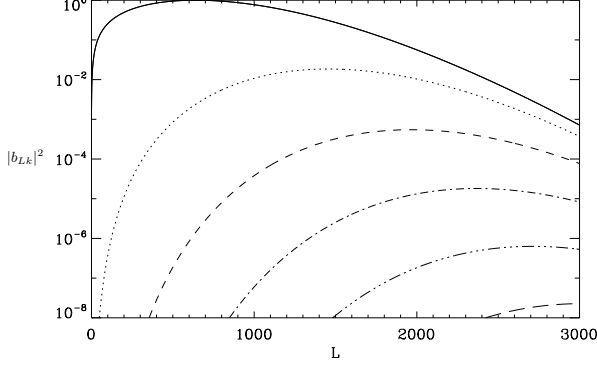


**Figure 2.** The amplitudes of the  $k=0, 2, 4, 6, 8, 10$  terms of the beam expansion,  $|b_{\ell k}|^2$ , as a function of multipole,  $\ell$ , for an elliptical Gaussian beam as defined in equation (50) with  $\sigma=3$  arcmin corresponding to a  $\theta_{\text{FWHM}}=7$  arcmin and ellipticity parameter,  $q=1.5$ .

once again, we can describe the beam asymmetry using a relatively small number of terms.

## 6.2 Using the noise power to set $k_{\text{max}}$ in a temperature only experiment

From the above demonstration, it appears that only a small number of terms in the harmonic expansion of the beam need to be retained in order to capture the global features of the beam response including the effects of asymmetry.

However, to be truly confident that the truncated expansion is an accurate enough representation of the beam, one would ideally choose the value of  $k_{\text{max}}$  such that the any residual error from misrepresenting the beam is smaller (to some tolerance level) than the statistical error in an experiment. For a particular asymmetric expansion term the leading order contribution to  $\tilde{C}_{\ell}^{00}$  is  $\sim |\tilde{b}_{0\ell k}|^2 C_{\ell}^{00}$ , where  $\tilde{b}_{0\ell k} = b_{0\ell k} \sqrt{\frac{4\pi}{2\ell+1}}$ . Therefore we can say that the asymmetric term should be included if

$$\langle p_k \rangle_{\text{pix}} |\tilde{b}_{0\ell k}|^2 C_{\ell}^{00} > f \langle N_{\ell}^{00} \rangle_{\sigma}, \quad (51)$$

where  $f$  is a tolerance level to which we require our systematic errors to be below the statistical error. A reasonable choice may be  $f=0.1$ , to ensure that the systematic error is 10% of the noise statistical error.  $\langle N_{\ell}^{00} \rangle_{\sigma}$  is the standard deviation of the noise power, see equation (31), which is the dominating source of statistical error at high  $\ell$ . The term  $\langle p_k \rangle_{\text{pix}}$  is the  $k^{\text{th}}$  mode of the  $\psi$  angle coverage quality of the scan strategy defined as

$$\langle p_k \rangle_{\text{pix}} = \left\langle \frac{1}{n_{\text{hits}}^2} \left| \sum_i e^{ik\psi_i} \right|^2 \right\rangle_{\text{pix}}, \quad (52)$$

where  $\langle \rangle_{\text{pix}}$  denotes an average over all pixels on the sky,  $n_{\text{hits}}$  is the number of hits a pixel receives and the sum over the index  $i$  is over all observations of a particular pixel. The lower the value of  $\langle p_k \rangle_{\text{pix}}$ , the better the scan strategy is at removing the bias created by the beam asymmetry due to the  $k^{\text{th}}$  azimuthal mode.

The rule of thumb in equation (51) becomes problematic when the sky coverage is small and in the presence of a highly asymmetric beam due to coupling between asymmetric terms of different  $k$ . This coupling is suppressed in the all-sky case because the cross spectra  $\mathcal{W}_{k_2 k_3}^{\ell}$  are small for  $k_2 \neq k_3$ , which in turn means the coupling matrix  $M_{00k_2 k_3}^{\ell_1 \ell_2}$  is small.

However in the case where the power in the mask extends to high  $\ell$  these cross spectra terms can become significant. This results in a significant contribution to the operator by a term of the form  $b_{0\ell_2 k_2}^* b_{0\ell_2 k_3} M_{00k_2 k_3}^{\ell_1 \ell_2}$ , where  $k_2 \neq k_3$ . This additional contribution could potentially be larger than the  $k_2 = k_3$  term if  $|b_{0\ell k_2}| \gg |b_{0\ell k_3}|$ .

## 7 TESTING THE PSEUDO- $C_{\ell}$ ON SIMULATIONS

In this section, we demonstrate the implementation of the pseudo- $C_{\ell}$  technique developed in Section 3 on numerical simulations of two representative types of CMB experiment – a generic balloon-borne experiment and a future satellite mission. Note that we test the performance of the algorithm in the temperature-only case. The implementation of our technique for polarization experiments will be presented in a future paper. For a temperature-only analysis, the coupling is reduced to

$$\tilde{C}_{\ell_1}^{00} = \sum_{\ell_2} O_{\ell_1 \ell_2}^{0000} C_{\ell_2}^{00} \quad \text{with}, \quad (53)$$

$$O_{\ell_1 \ell_2}^{0000} = \sum_{k_2 k_3} b_{0\ell_2 k_2}^* b_{0\ell_2 k_3} M_{00k_2 k_3}^{\ell_1 \ell_2} \quad (54)$$

The main stages of the simulation pipeline are as follows:

- (i) We use the HEALPix package to create simulations of the CMB temperature field based on the theoretical CMB power spectrum for the concordance  $\Lambda$ CDM cosmological model.
- (ii) We then create a TOD by convolving the CMB with the telescope beam in the appropriate orientation given the scan strategy.
- (iii) We then calculate the  $\tilde{C}_{\ell}^{00}$  using equation (16).
- (iv) The coupling operator is calculated using the expression in equation (54).
- (v) With the operator  $O_{\ell_1 \ell_2}^{0000}$  calculated, we then invert it to recover an estimate of the full-sky and beam-deconvolved power spectrum.

Note that we use two different convolution codes for the two classes of experiment that we simulate. For the balloon-like test we calculate each element of the TOD using equation (10). The HEALPix ROTATE\_ALMS routine operates on the beam multipole coefficients. This function uses the Wigner D-matrices to rotate the beam coefficients by a set of Euler angles given on input. The TOD element can then be calculated using,

$$t_j = \sum_{lm} b_{lm}^{j*} a_{lm}, \quad (55)$$

where  $b_{lm}^{j*}$  is the multipole expansion of the beam when it has been rotated through the Euler angles  $\omega_j$ . In this way the whole TOD can be created. While this is accurate and simple it would be impossible to use this approach in the satellite-like experiment as the number of TOD elements and the required  $\ell_{\text{max}}$  would make it computationally infeasible. To create the simulated TOD in the satellite-like case, we use a method similar to the FEBeCoP approach (Mitra et al. 2011) except that do not calculate the effective beams but rather we produce the individual TOD elements. The convolution is simplified by describing the beam in pixel space and we only calculate the value of the beam on a set of neighbouring pixels centred around the pointing centre of the beam. We use pixels within  $5\sigma q$  of the centre of the beam (see equation 50) to describe the beam over this localised region of sky.

A second technical challenge was to obtain the Wigner D-matrix transforms of the TOD and the window function. We achieved this by implementing equations (13) and (14) using the



expression for the Wigner D-matrix in terms of spin weighted spherical harmonics (equation 17). First, the integral over  $\psi$  was performed using a simple Newton-Cotes numerical integration method. The HEALPix routine MAP2ALM\_SPIN was then used to perform the integrals over  $\theta$  and  $\phi$ .

### 7.1 Balloon-like experiment

For our first test we use the simulated LSPE beam shown in Fig. 1 with a modification. We greatly amplify the size of the asymmetry in order to produce a more stringent test of the asymmetry correction algorithm. The spherical harmonic decomposition of this exaggerated beam is related to the original LSPE decomposition by

$$b_{0\ell,k}^{\text{exagg}} = b_{0\ell,0}^{\text{LSPE}} \delta_{k0} + b_{0\ell,\pm 2}^{\text{LSPE}} \delta_{k\pm 2} \times 100. \quad (56)$$

We use the planned scan strategy for LSPE but we stress that we have not included the effects of the half-wave plate (HWP) that LSPE will use. The LSPE experiment will incorporate a HWP in front of the optics which will be used to increase the polarization angle coverage of the experiment. However, for the purposes of this demonstration where we consider a temperature-only experiment, we have ignored the (advantageous) effects of the HWP. LSPE will be launched at a latitude of  $78^\circ$  North and will follow a jet stream around the globe staying at roughly the same latitude. The payload will spin at 3 rpm and the telescope will perform constant altivation scans with regular ( $\S$ daily) steps in elevation (The LSPE collaboration et al. 2012).

We created a set of TOD following the above procedure including white noise. The LSPE scan strategy covers  $\sim 25\%$  of the sky and so provides a test of the algorithm's ability to account for a cut sky in addition to the effects of beam asymmetry. Fig. 3 shows an example of a simple binned map created from one of our simulations. This figure also shows the hit map of the scan strategy, the  $2^{\text{nd}}$   $\psi$  coverage quality  $p_2$  defined in Section 6.2 and the weighting function that we use to apodise the hit map. We include an (unrealistically high) noise level of 1.6 mK-arcmin in our simulations in order to test the removal of noise bias from the recovered power spectrum.

The  $\tilde{C}_\ell^{00}$  for 1000 realisations were computed according to equation (53) and the coupling operator was calculated using equation (54). In order to invert the coupling matrix we needed to bin the  $\tilde{C}_\ell^{00}$  and the coupling operator, as in Hivon et al. (2002). This binning ensures that the matrix is invertible and that the resulting data points are uncorrelated. Here we use a bin size of  $\Delta\ell=20$ . A correction for noise bias was also implemented following the procedure outlined in Section 3.4. Fig. 4 shows the mean power spectrum recovered from the simulations in comparison to the input spectrum. In this figure, we also plot the mean power spectrum recovered when the beam was assumed to be axisymmetric, by including only the  $b_{0\ell 0}$  term on the pseudo- $C_\ell$ . This figure clearly demonstrates that our algorithm can successfully recover the power spectrum in a situation where the axisymmetric approximation clearly fails. The power spectrum obtained in the case where the noise in the TOD was ignored is also shown demonstrating the ability of our algorithm to successfully correct for noise bias.

### 7.2 Satellite-like experiment

The second test that we perform is using a satellite-like scan strategy. For this test, we use a beam described by equation (50) with

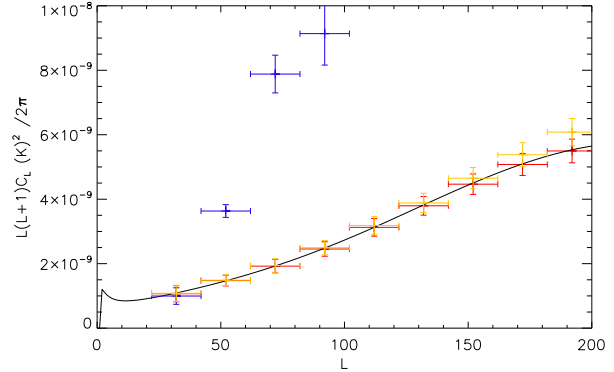


**Figure 4.** Reconstruction of the power spectrum for the balloon-like simulation using the pseudo- $C_\ell$  method. The input theoretical power spectrum is plotted (black) along with the recovered power spectrum when the exaggerated beam is used (red), averaged over 1000 realisations. We also plot the recovered power spectrum one would recover if the axisymmetric MASTER (Hivon et al. 2002) analysis was used (blue) and if the noise was ignored (yellow). The vertical error bars show the standard deviation of the realisations from the mean.

$\sigma=3$  arcmin corresponding to a FWHM of 7 arcmin and  $q=1.5$ . The scan strategy used is similar to that proposed for the Experimental Probe of Inflationary Cosmology (EPIC, Bock et al. 2009). In Fig. 5 we show the hit map, the  $p_2$  quality (equation 52) and the weighting function that we have used to mask the galaxy and extragalactic sources. We use the same mask as was used by the Planck collaboration (Planck Collaboration et al. 2013b) for their power spectrum analysis. The weighting function also apodises the hit map. Note that the EPIC scan strategy was designed to improve the  $2^{\text{nd}}$   $\psi$  coverage quality defined in Section 6.2. This choice of scan strategy will therefore be effective in mitigating beam asymmetries even in the absence of a dedicated correction algorithm. We therefore expect the bias, in the absence of a dedicated correction, to be much smaller than seen in the previous section (although it will still be non-zero). The mean recovered power spectra using  $k_{\text{max}}=0, 2$  are shown in the top panel of Fig. 6. The lower panel of this figure shows the fractional residual bias in the power spectrum recovery and demonstrates an unbiased result to high- $\ell$  when  $k_{\text{max}}=2$  is used. These simulations included white noise such that the error on the map is equivalent to  $8.5 \mu\text{K-arcmin}$ . We can see that even with a scan strategy designed to optimise crossing angles and thereby reduce the asymmetry bias, there remains a bias at the level of  $\sim 1-2\sigma$  when the axisymmetric approximation is made.

The importance of this test is two-fold. It demonstrates that the algorithm can deal with a more conventional elliptical Gaussian beam and also that it can be extended to high- $\ell$ . The coupling operator was calculated in 9 hrs on one 2.26 GHz processor to  $\ell_{\text{max}} = 4000$ . We calculated the coupling operator to a much higher  $\ell$  than the maximum multipole of interest to ensure that we did not miss any effects from the aliasing of power from higher multipoles.

## 8 TESTING THE MAP-MAKING ALGORITHM ON SIMULATIONS

We test the map-making algorithm described in Section 5 in two ways. First, we use the algorithm on multiple realisations of the same simulated experiment as described in Section 7.2 to show that

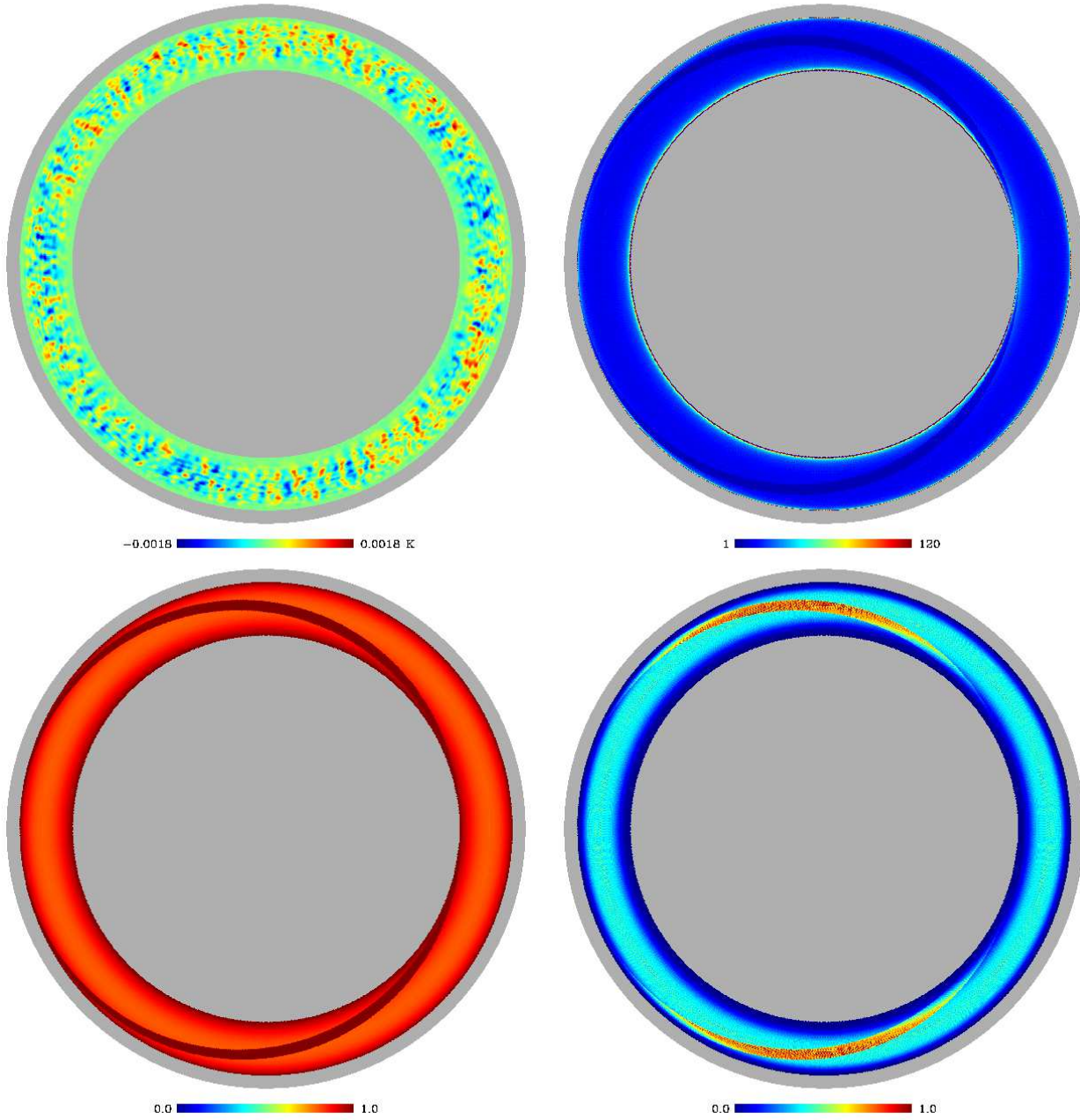


**Figure 3.** *Top left:* An example binned map made in the balloon-like test. The exaggerated beam was used with a spherical harmonic decomposition as described in equation (56). The scan strategy implemented is typical of a balloon based experiment. *Top right:* The hit map from one day of observations for the balloon-like experiment. *Bottom left:* The  $p_2$  quality, defined in equation (52), of the scan strategy. We note again that a HWP was not included which is why the polarization angle coverage is poor for this simulation. *Bottom right:* The weighting function applied to apodise the hit map.

the algorithm can correctly remove the asymmetry bias on the temperature power spectrum. The second test is performed on a single noise-free full sky simulation of the satellite experiment. We use this latter simulation to test if the algorithm can successfully remove the asymmetry bias directly from the temperature and polarisation maps. We do not include a CMB polarisation signal in our TOD and so a successful asymmetry correction algorithm should recover a zero polarisation signal.

### 8.1 Removing the asymmetry bias on the temperature power spectrum

As in Section 7.2, we create 48 TOD realisations using the satellite-like scan strategy, and using an elliptical Gaussian beam with  $\theta_{\text{FWHM}}=7$  arcmin and  $q=1.5$  (see equation 50). As before, the TOD included white noise equivalent to a map noise level of  $8.5 \mu\text{K}$  arcmin.

From the simulated TOD, we then compute both a simple binned map and a map constructed using the algorithm presented in Section 5 with  $k_{\text{max}}=2$ . We then apply the same galactic and point source mask to these maps as used in Section 7.2. A stan-

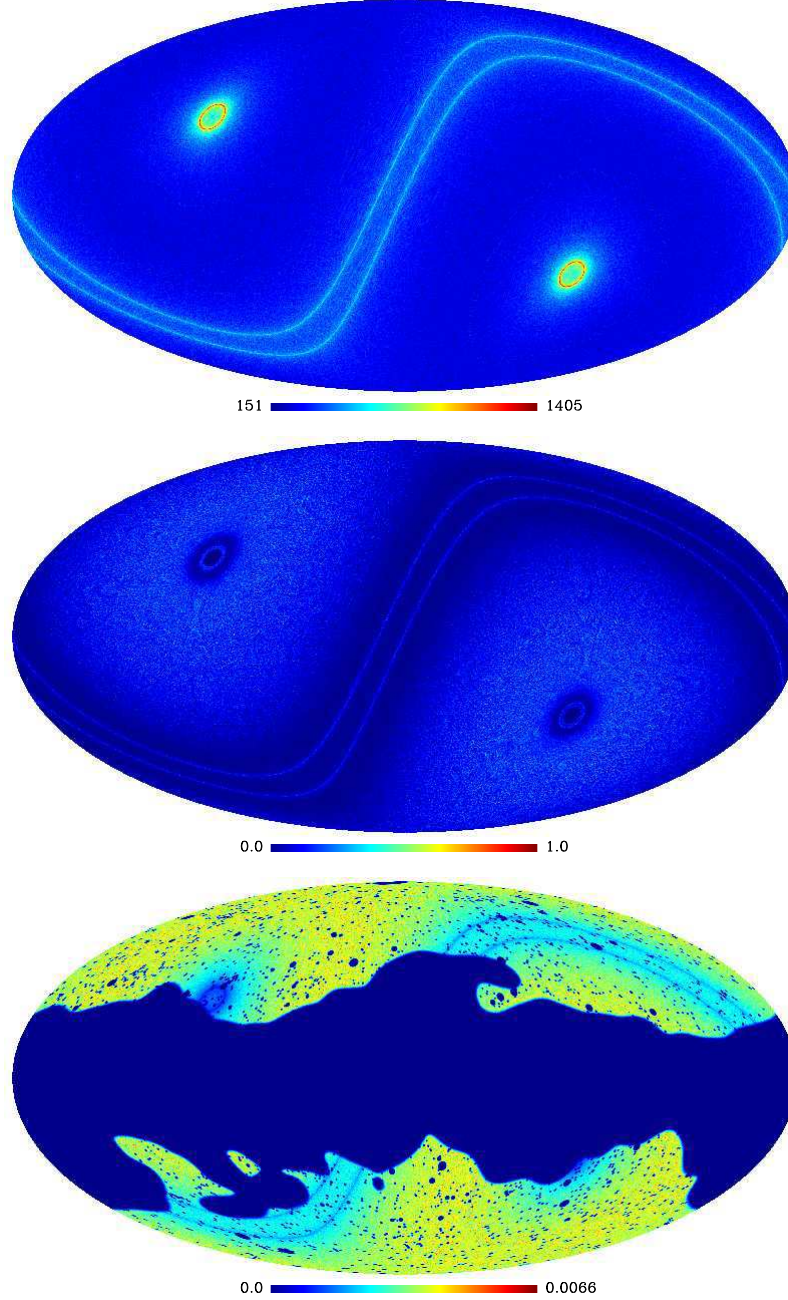


**Figure 5.** *Top panel:* The hit map for one year of observations for our simulated satellite-like experiment. *Middle:* The  $p_2$  quality, defined in equation (52), of the scan strategy. *Bottom panel:* The weighting function used to apply a galactic and point source mask and apodise the hit map.

dard pseudo- $C_\ell$  analysis (Hivon et al. 2002) is then applied in order to recover the power spectrum. The recovered power spectrum is then deconvolved by dividing by the beam window function  $B_\ell = \sqrt{\frac{4\pi}{2\ell+1}} b_{0\ell 0}$ , which is the axisymmetric component of the input beam. Fig. 7 shows the recovered power spectrum for the binned map and for the asymmetry cleaned map obtained using the new map-making algorithm of Section 5. The asymmetry bias has clearly been removed successfully. Note that the removal of the asymmetry bias comes at the cost of a modest inflation of the power spectrum error-bars which have increased by  $\sim 20\%$ . This increased error is modest compared to the systematic bias that has been removed.

## 8.2 Removing the asymmetry bias on the temperature and polarisation maps

Here we present a demonstration of how the map-making algorithm can be used to remove the asymmetry bias on both the temperature and polarisation maps.

To estimate the temperature map, the algorithm of Section 5 extracts only the spin-0 components of the TOD. This quantity contains the temperature of the CMB smoothed with the axisymmetric component of the beam. To demonstrate this we simulate a noise free TOD using the elliptical Gaussian and the satellite-like scan strategy. We plot the CMB used in the simulation smoothed with the axisymmetric component of the beam in the top panel of Fig. 8.



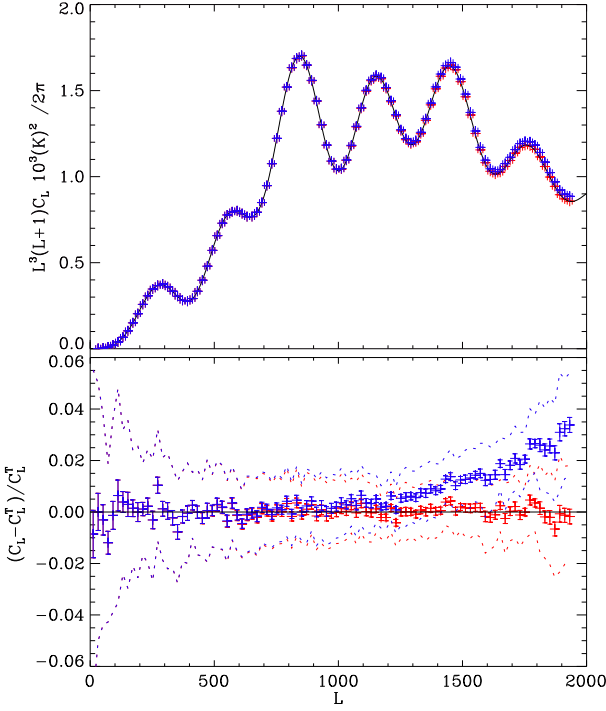


**Figure 6.** Reconstruction of the power spectrum for the satellite-like simulation using the pseudo- $C_\ell$  method. *Top:* The input theoretical power spectrum is plotted (black) along with the recovered power spectrum for  $k_{\max}=0, 2$  (blue and red points respectively) averaged over 48 realisations. *Bottom:* The fractional error between the recovered band powers and the binned input power spectrum. The error bars show the statistical error on the recovered mean, while the dashed lines show the  $1\sigma$  error that would be seen in a real experiment. We see that the  $k_{\max}=2$  recovery is unbiased to a small fraction of the statistical error caused by noise.

The other three panels in this figure show the absolute error between this isotropically smoothed map and a simple binned map (second panel); and between the isotropically smoothed map and maps produced using the map-making algorithm with  $k_{\max}=2$  and  $k_{\max}=4$  (lower two panels). The reduction in the bias due to beam asymmetry as  $k_{\max}$  is increased is clearly demonstrated by this figure.

We also tested the ability of the map-making algorithm to remove the leakage from temperature to polarisation due to the asymmetry of the beam. We performed this test using the approach described in Section 5.2 which makes use of a previously estimated temperature map obtained with the method described in Section 5.1 with  $k_{\max}=4$ . In our simulation we have not included an input polarisation signal so the expected power in the polarisation maps will be zero in the absence of systematics. As described in Section 4, the temperature to polarization leakage could contaminate either the  $E$ -mode or the  $B$ -mode power spectrum depending on the relative orientation between the beam ellipticity and the polarisation response of the detector.

In Fig. 9 we plot the power of the leaked temperature to polarisation signal and the power in the polarization maps after this leakage has been removed using the approach described in Section 5.2. The power in the cleaned polarisation map has been successfully reduced by  $\sim 4$  orders of magnitude compared to the uncleaned map.

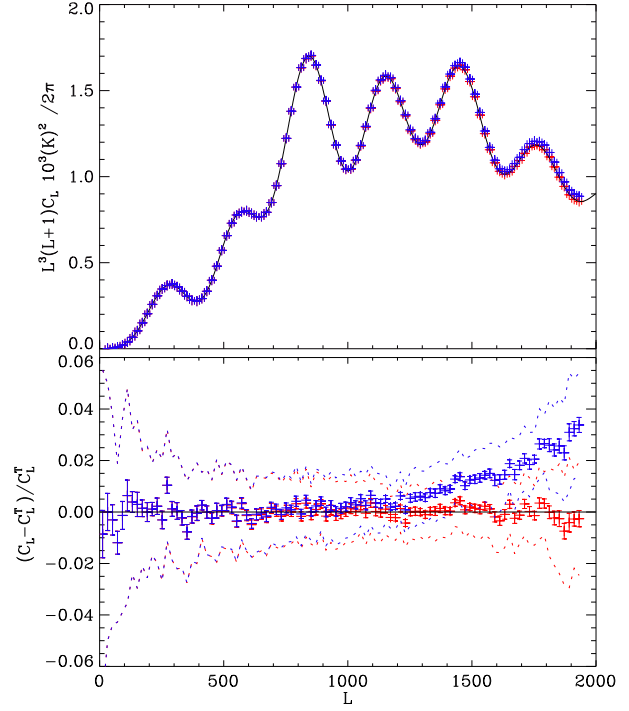


**Figure 7.** Reconstruction of the power spectrum for the satellite-like simulation using the map-making method. This should be compared to Fig. 6 which presents the results of the pseudo- $C_\ell$  method. *Top:* The input theoretical power spectrum is plotted (black) along with the recovered bandpowers for the binned map (blue points), and where the map-making algorithm is used with  $k_{\max}=2$  (red points), averaged over 48 realisations. *Bottom:* The fractional error between the recovered bandpowers and the binned input power spectrum. The error bars show the statistical error on the recovered mean, while the dashed lines show the  $1\sigma$  error that would be achieved by a single experiment. We see that the map-making technique using  $k_{\max}=2$  produces power spectrum estimates that are unbiased to a small fraction of the statistical error caused by noise.

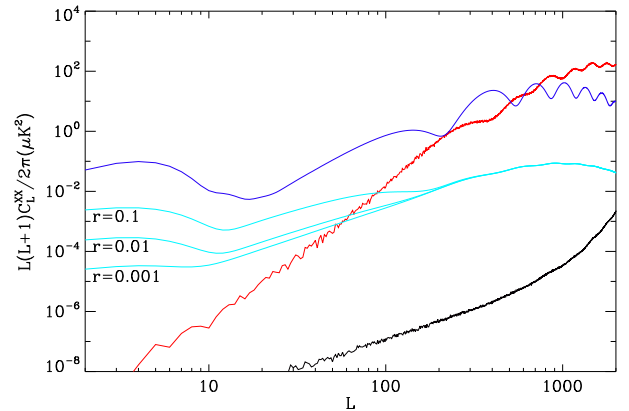


**Figure 9.** The power spectrum of the temperature signal leaked to polarization as a result of beam asymmetries for the simulated satellite-like experiment (red). This power could manifest itself as either an  $E$ -mode, a  $B$ -mode or a combination of both – see the discussion in Section 4. The black line shows the power spectrum of the polarisation leakage after applying the correction algorithm described in Section 5.2. For comparison we plot the expected  $E$ -mode and  $B$ -mode signal in dark and light blue respectively. The expected  $B$ -mode signal is plotted for three cases of the tensor-to-scalar ratio:  $r=0.001, 0.01, 0.1$ .



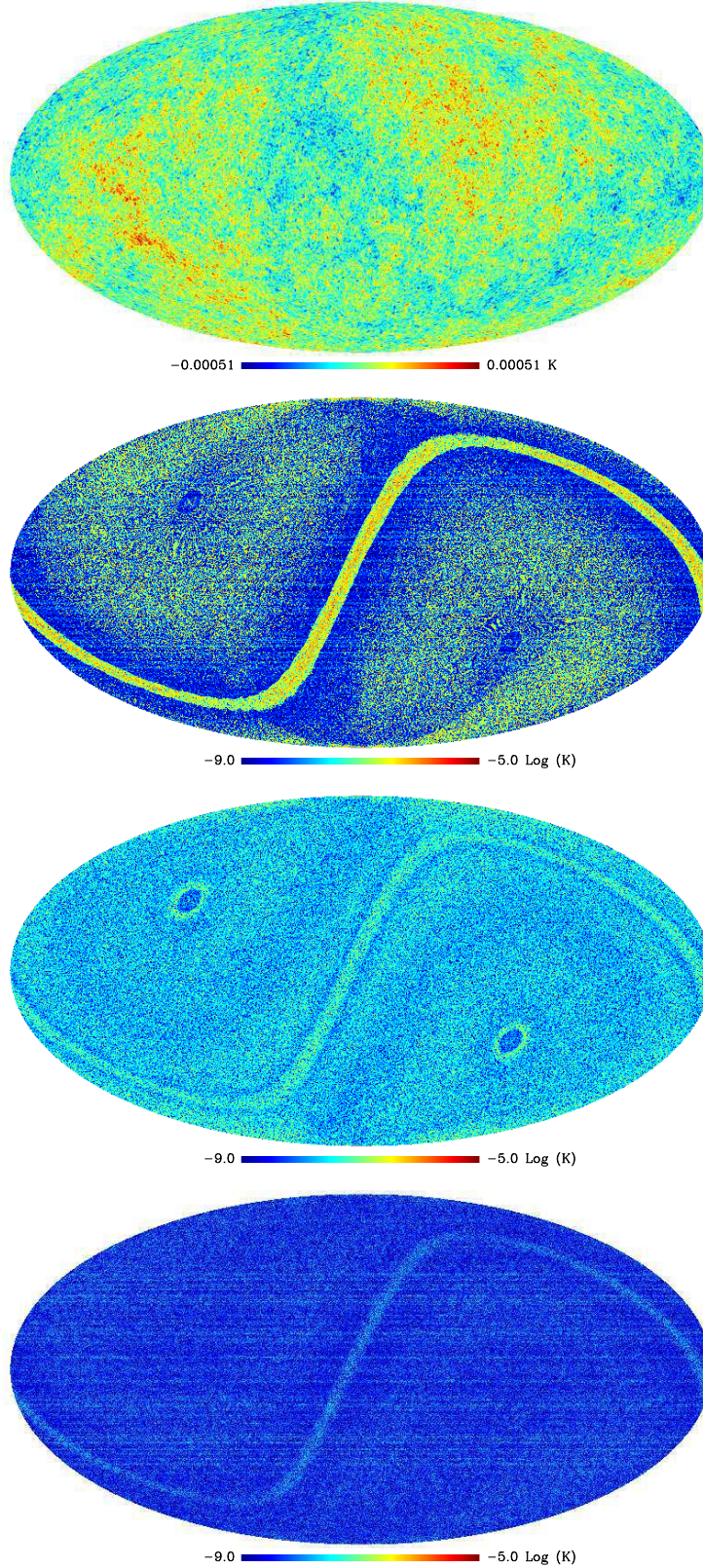


**Figure 8.** *Top panel:* The input CMB realization directly convolved with the axisymmetric component of the elliptical Gaussian beam used for the satellite-like simulation. *Second panel:* The absolute residuals between the isotropically smoothed map shown in the top panel and the simple binned map constructed from the simulated TOD. *Lower two panels:* The absolute residuals between the isotropically smoothed map shown in the top panel and maps made using the algorithm described in Section 5 with  $k_{\max}=2$  and  $k_{\max}=4$ . The residuals in the  $k_{\max}=4$  case (*bottom panel*) are comparable with the numerical noise of our convolution code.

## 9 DISCUSSION

We have developed two separate techniques to remove asymmetry bias in CMB experiments. The first is a pseudo- $C_\ell$  method that corrects for the asymmetry bias on the temperature and polarisation power spectra. There is no assumption on the scan strategy and only a modest approximation to the beam is required. The analysis is similar to the MASTER algorithm (Hivon et al. 2002) and its extension to polarisation (Brown, Castro, & Taylor 2005). However we include additional contributions to the coupling operator that corrects for the contaminating effects of the beam asymmetry. We note that this algorithm can only be applied to experiments that can directly measure the  $Q$  and  $U$  Stokes parameters in the timeline, e.g. a differencing experiment with both instrument- $Q$  and instrument- $U$  detectors on its focal plane. This is due to the fact that we make no attempt to make a map and so we must have measurements of the Stokes parameters in the telescope’s frame of reference. At present the formalism assumes the four beams required for such a differencing experiment are the same. In future work we will relax this assumption.

Using this formalism we also examined the inter-spectra coupling resulting from the beam asymmetry. As an example, we investigated the coupling between temperature and B-mode power in the presence of an ideal scan strategy. In doing so we showed that the temperature power will be coupled to the B-mode power if the beam asymmetry is at an angle to the polarisation sensitivity direction of the detector. This result is in agreement with previous work (Shimon et al. 2008).

The coupling operator in equation (24) allows us to calculate the contribution to each pseudo- $C_\ell$  from the sky power, due to both the mask and beam asymmetry. By inverting this operator we can, therefore, calculate an unbiased estimate for the CMB power spectra. To calculate the operator  $\mathbf{O}_{i_1 i_2}$  we must cap the azimuthal dependence of the beam,  $k_{\max} \lesssim 10$ . We demonstrated in Section 6, and in Figs. 1 and 2, that a simulated beam from a multi-moded horn, and an elliptical Gaussian, equation (50), are both well described by only a few azimuthal modes. This property allows us to remove to a high degree of accuracy the bias due to the beam asymmetry for any given scan strategy.

We then went on to implement this algorithm in the temperature only case for two simulated experimental set-ups: a balloon-like experiment and a satellite-like experiment. We showed that we could successfully recover the input power spectrum, when the TOD was created using a highly asymmetric beam in the presence of both a severe sky-cut and instrument noise. These tests showed that the algorithm can deal comfortably with beams that have much higher levels of asymmetry than that typically found in real CMB experiments, and using two completely different and realistic scan strategies. The scan strategies investigated include the proposed scanning mode for the forthcoming balloon-borne LSPE experiment (The LSPE collaboration et al. 2012), and a scan strategy optimized for a possible future CMB polarization satellite mission (Bock et al. 2009).

The second technique that we propose for removing beam asymmetry bias is a new map-making algorithm. The map-making algorithm produces temperature and polarisation maps of the CMB that are smoothed with only the axisymmetric component of the beam. It achieves this by separating out the different spin components of the detected signal using equation (42). This allows us to obtain unbiased estimates for the spin-0 and spin-2 components of the signal which correspond to the temperature and polarisation of the pixel. The temperature map estimated using this technique will

be clean of systematics due to the asymmetry of the beam. However, the polarisation map will still contain a temperature to polarisation leakage term due to the  $k=2$  azimuthal mode of the beam. This contaminating signal can effectively be removed by calculating the leakage from the estimated temperature map and the known beam response as described in Section 5.2.

Removing the effects of beam asymmetry at the map level is preferable to removing it using the pseudo- $C_\ell$  method. There are three main reasons for this. Firstly there will be no aliasing between spectra. By removing the inter-spectra leakage at the power spectrum level we will increase the statistical error on the recovered power spectra by a factor proportional to the amplitude of the leaked spectra. A more optimal estimate of the true power spectrum can therefore be obtained if we can remove the leakage in the map domain. Secondly, the map-making algorithm can be applied before foregrounds are removed, allowing the application of traditional foreground removal techniques on the beam asymmetry-cleaned maps. Thirdly, the cleaned maps can subsequently be used for other science applications beyond the power spectrum such as CMB lensing, non-Gaussianity studies and foreground science. Note error propagation from uncertainty in the beam shape may be more complicated. We propose that an experiment should Monte-Carlo over uncertainties in the beam to be able to fully understand the errors on the map and therefore the science.

The map-making algorithm requires a scan strategy to cross a pixel at multiple orientations. If this is not the case, the matrix  $H_{kk'}$ , defined in equation (41), is not invertible. In such cases, the map-making method cannot be applied (although the pseudo- $C_\ell$  approach could still be used). We note that, as an alternative to a highly redundant scan strategy, the required polarisation angle coverage could also be provided through the use of an appropriately positioned HWP, as is the case in the LSPE experiment (The LSPE collaboration et al. 2012).

In Section 8 we showed that we could use the map-making algorithm to correctly recover an input temperature power spectrum free of asymmetry bias for the same simulated satellite-like experiment as was used to test the pseudo- $C_\ell$  technique. In doing this we found that the noise level in the recovered power spectrum increased by  $\sim 20\%$  compared to that recovered from a simply binned map. We also demonstrated that we could successfully correct the temperature and polarisation signal for the effects of beam asymmetry at the map level. To demonstrate this, we simulated a satellite-like experiment free of noise and we computed the temperature and polarisation maps using the algorithm described in Section 5. For the case of  $k_{\max}=4$  we showed that the residual error between the resulting estimated temperature map and the input temperature map smoothed with the axisymmetric component of the beam was comparable to the numerical error in the convolution code. Finally, we have also demonstrated that this method could be very powerful for correcting for temperature to polarization leakage due to beam asymmetries. This ability, which is demonstrated in Fig. 9, could prove extremely useful for controlling systematics due to beam asymmetries in future precision CMB  $B$ -mode polarization experiments.

## ACKNOWLEDGMENTS

CGRW acknowledges the award of a STFC quota studentship. MLB is grateful to the European Research Council for support through the award of an ERC Starting Independent Researcher Grant (EC FP7 grant number 280127). MLB also thanks the STFC

for the award of Advanced and Halliday fellowships (grant number ST/I005129/1). We also thank Bruno Maffei and the LSPE collaboration for helpful discussions. Some of the results in this paper have been derived using the HEALPix (Górski et al. 2005) package.

## REFERENCES

- Bischoff C., BICEP Collaboration, 2013, IAUS, 288, 61
- Bock J., et al., 2009, arXiv, arXiv:0906.1188
- Brown M. L., Castro P. G., Taylor A. N., 2005, MNRAS, 360, 1262
- Brown M. L., et al., 2009, ApJ, 705, 978
- Buder I., BICEP Collaboration, 2013, AAS, 222, #103.01
- Challinor A., 2013, IAUS, 288, 42
- Challinor A., Fosalba P., Mortlock D., Ashdown M., Wandelt B., Górski K., 2000, PhRvD, 62, 123002
- Chiang, H. C., Ade, P. A. R., Barkats, D., et al. 2010, ApJ, 711, 1123
- Goldberg J. N., Macfarlane A. J., Newman E. T., Rohrlach F., Sudarshan E. C. G., 1967, JMP, 8, 2155
- Górski, K. M., Hivon, E., Banday, A. J., et al. 2005, ApJ, 622, 759
- Hanson, D., Hoover, S., Crites, A., et al. 2013, Physical Review Letters, 111, 141301
- Hanson D., Lewis A., Challinor A., 2010, PhRvD, 81, 103003
- Hivon E., Górski K. M., Netterfield C. B., Crill B. P., Prunet S., Hansen F., 2002, ApJ, 567, 2
- Keihänen E., Reinecke M., 2012, A&A, 548, A110
- Kovac, J. M., Leitch, E. M., Pryke, C., et al. 2002, Nature, 420, 772
- The LSPE collaboration, et al., 2012, arXiv, arXiv:1208.0281
- Mitra S., Rocha G., Górski K. M., Huppenberger K. M., Eriksen H. K., Ashdown M. A. J., Lawrence C. R., 2011, ApJS, 193, 5
- Montroy, T. E., Ade, P. A. R., Bock, J. J., et al. 2006, ApJ, 647, 813
- O’Dea D., Challinor A., Johnson B. R., 2007, MNRAS, 376, 1767
- Planck Collaboration, et al., 2013a, arXiv, arXiv:1303.5062
- Planck Collaboration, et al., 2013b, arXiv, arXiv:1303.5068
- Planck Collaboration, et al., 2013c, arXiv, arXiv:1303.5076
- Polarbear Collaboration, et al., 2013, arXiv, arXiv:1312.6646
- QUIET Collaboration, et al., 2012, arXiv, arXiv:1207.5562
- Ramamonjisoa F. A., Ray S., Mitra S., Souradeep T., 2013, arXiv, arXiv:1309.4784
- Readhead, A. C. S., Myers, S. T., Pearson, T. J., et al. 2004, Science, 306, 836
- Shimon M., Keating B., Ponthieu N., Hivon E., 2008, PhRvD, 77, 083003
- Souradeep T., Mitra S., Sengupta A., Ray S., Saha R., 2006, NewAR, 50, 1030
- Wandelt B. D., Górski K. M., 2001, PhRvD, 63, 123002
- Varshalovich, D., Moskalev, A., Khersonskii, V., 1988. Quantum theory of angular momentum. World Scientific Publishing Co. Inc.



**APPENDIX A: RELATIONSHIP BETWEEN OUR PSEUDO- $C_\ell$  AND THE STANDARD PSEUDO- $C_\ell$** 

Here we show that the pseudo- $C_\ell$  expression derived in Section 3 reduces to a rewriting of the standard polarised pseudo- $C_\ell$  presented in Brown, Castro, & Taylor (2005), in the case where the beam is axisymmetric and where the experiment has both instrument- $Q$  and instrument- $U$  detectors. We begin by looking at the coupling kernel,

$$K_{m_1 k_1 m_2 k_2}^{\ell_1 \ell_2} \equiv \int d^3 \omega D_{m_1 k_1}^{\ell_1}(\omega) D_{m_2 k_2}^{\ell_2*}(\omega) W(\omega) n(\omega). \quad (\text{A1})$$

$$(\text{A2})$$

We use the weighting function  $n(\omega)$  to apodise the hit map and apply a galactic mask. While, in general, it can be a function of  $\theta$ ,  $\phi$  and  $\psi$ , in practice, it is sufficient for it to be a function of just  $\theta$  and  $\phi$ . The function will be discretised. It should be chosen such that  $\int d\psi W(\omega) n(\theta, \phi)$  for a given pixel ranges from 0 to 1 and acts as the standard window function in the pseudo- $C_\ell$ . The requirement that the experiment has both an instrument- $Q$  and - $U$  detector means that for every orientation of the telescope  $\omega$  we have 4 detections of the sky each at  $[\theta, \phi, \psi + j\pi/4]$ , where  $j=0,1,2,3$ . A consequence of this arrangement of detectors is that

$$\int d\psi W(\omega) e^{ik\psi} = 0 \quad \text{for } k = \pm 2, \pm 4. \quad (\text{A3})$$

Therefore  $K_{m_1 k_1 m_2 k_2}^{\ell_1 \ell_2} = 0$  if  $k_1 - k_2 = \pm 2, \pm 4$ . We can now examine the Wigner decomposition of the time stream, in particular the  $k=0, \pm 2$  components, as these will contain information on the temperature and polarisation of the CMB. We also assume the beam to be axisymmetric and have a zero cross polar response, so that  $b_{s\ell k} = 0$  for  $s \neq -k$ . We make this assumption in order to make the connection with the standard pseudo- $C_\ell$  approach. Applying these constraints to equation (18) we get,

$$T_{m_1 0}^{\ell_1*} = \sum_{\ell_2 m_2} b_{0\ell_2 0}^* a_{0\ell_2 m_2} K_{m_1 0 m_2 0}^{\ell_1 \ell_2} \quad (\text{A4})$$

$$T_{m_1 \pm 2}^{\ell_1*} = \sum_{\ell_2 m_2} b_{\mp 2\ell_2 \pm 2}^* a_{\mp 2\ell_2 m_2} K_{m_1 \pm 2 m_2 \pm 2}^{\ell_1 \ell_2}. \quad (\text{A5})$$

Using these expressions, we can show that  $E$ - and  $B$ -mode-like decompositions (equations 33 & 34) of the TOD in this experiment will be,

$$\begin{aligned} T_{m_1 E}^{\ell_1*} &= \sum_{\ell_2 m_2} b_{-2\ell_2 2}^* \left( a_{\ell_2 m_2}^E K_{\ell_1 \ell_2 m_1 m_2}^+ + a_{\ell_2 m_2}^B K_{\ell_1 \ell_2 m_1 m_2}^- \right) \\ T_{m_1 B}^{\ell_1*} &= \sum_{\ell_2 m_2} b_{-2\ell_2 2}^* \left( a_{\ell_2 m_2}^B K_{\ell_1 \ell_2 m_1 m_2}^+ - a_{\ell_2 m_2}^E K_{\ell_1 \ell_2 m_1 m_2}^- \right), \end{aligned} \quad (\text{A6})$$

where we have defined,

$$K_{\ell_1 \ell_2 m_1 m_2}^+ \equiv -\frac{1}{2} \left( K_{m_1 2 m_2 2}^{\ell_1 \ell_2} + K_{m_1 -2 m_2 -2}^{\ell_1 \ell_2} \right) \quad (\text{A7})$$

$$K_{\ell_1 \ell_2 m_1 m_2}^- \equiv \frac{i}{2} \left( K_{m_1 2 m_2 2}^{\ell_1 \ell_2} - K_{m_1 -2 m_2 -2}^{\ell_1 \ell_2} \right). \quad (\text{A8})$$

Comparing the expressions of equation (A6) with equation (10) of Brown, Castro, & Taylor (2005) shows that the  $E$ - and  $B$ -mode-like decompositions of the TOD defined in equations (33) & (34) have a similar form to the  $E$ - and  $B$ -mode decompositions of a polarisation map used in the standard pseudo- $C_\ell$  technique. They are similar in the sense that they are both the sky polarisation smoothed with the beam, and then convolved with a window function. They differ only in normalisation factors. As the decompositions are similar, the pseudo- $C_\ell$  constructed from them will also be similar.

**APPENDIX B: PRODUCT OF TWO COUPLING KERNELS**

We require the product of two coupling kernels. In order to calculate this, we start from the definition the Kernel

$$K_{m_1 k_1 m_2 k_2}^{\ell_1 \ell_2} \equiv \int d^3 \omega D_{m_1 k_1}^{\ell_1}(\omega) D_{m_2 k_2}^{\ell_2*}(\omega) W(\omega) n(\omega) \quad (\text{B1})$$

$$= \sum_{\ell_3 m_3 k_3} w_{m_3 k_3}^{\ell_3} \int d^3 \omega D_{m_1 k_1}^{\ell_1}(\omega) D_{m_2 k_2}^{\ell_2*}(\omega) D_{m_3 k_3}^{\ell_3}(\omega) \quad (\text{B2})$$

$$= 8\pi^2 (-1)^{m_2+k_2} \sum_{\ell_3 m_3 k_3} w_{m_3 k_3}^{\ell_3} \begin{pmatrix} \ell_1 & \ell_2 & \ell_3 \\ m_1 & -m_2 & m_3 \end{pmatrix} \begin{pmatrix} \ell_1 & \ell_2 & \ell_3 \\ k_1 & -k_2 & k_3 \end{pmatrix}, \quad (\text{B3})$$



where the second equality comes from an identity found in Varshalovich et al. (1988). We can now evaluate the product summed over certain indices  $m_1$ , and  $m_2$

$$M_{k_1 k'_1 k_2 k_3}^{\ell_1 \ell_2} \equiv \sum_{m_1 m_2} K_{m_1 k_1 m_2 k_2}^{\ell_1 \ell_2} K_{m_1 k'_1 m_2 k_3}^{\ell_1 \ell_2 *} \quad (\text{B4})$$

$$= 64\pi^4 (-1)^{k_2+k_3} \sum_{\substack{m_1 m_2 \\ \ell_4 m_4 k_4 \\ \ell_5 m_5 k_5}} w_{m_4 k_4}^{\ell_4} w_{m_5 k_5}^{\ell_5 *} \begin{pmatrix} \ell_1 & \ell_2 & \ell_4 \\ m_1 & -m_2 & m_4 \end{pmatrix} \begin{pmatrix} \ell_1 & \ell_2 & \ell_4 \\ k_1 & -k_2 & k_4 \end{pmatrix} \\ \times \begin{pmatrix} \ell_1 & \ell_2 & \ell_5 \\ m_1 & -m_2 & m_5 \end{pmatrix} \begin{pmatrix} \ell_1 & \ell_2 & \ell_5 \\ k'_1 & -k_3 & k_5 \end{pmatrix}. \quad (\text{B5})$$

The Wigner  $3j$  orthogonality relation is

$$\sum_{m_1 m_2} \begin{pmatrix} \ell_1 & \ell_2 & \ell_4 \\ m_1 & m_2 & m_4 \end{pmatrix} \begin{pmatrix} \ell_1 & \ell_2 & \ell_5 \\ m_1 & m_2 & m_5 \end{pmatrix} = \frac{1}{2\ell_4 + 1} \delta_{\ell_4, \ell_5} \delta_{m_4, m_5}, \quad (\text{B6})$$

which enables the sum over  $m_1$  and  $m_2$  to be performed and evaluating the Kronecker  $\delta$  gives

$$M_{k_1 k'_1 k_2 k_3}^{\ell_1 \ell_2} = 64\pi^4 (-1)^{k_2+k_3} \sum_{\ell_4 m_4 k_4 k_5} w_{m_4 k_4}^{\ell_4} w_{m_4 k_5}^{\ell_4 *} \frac{1}{2\ell_4 + 1} \begin{pmatrix} \ell_1 & \ell_2 & \ell_4 \\ k_1 & -k_2 & k_4 \end{pmatrix} \begin{pmatrix} \ell_1 & \ell_2 & \ell_4 \\ k'_1 & -k_3 & k_5 \end{pmatrix}. \quad (\text{B7})$$

We can simplify this further by defining the window correlation matrix  $\mathcal{W}_{k_1, k_2}^{\ell} \equiv \sum_m w_{m k_1}^{\ell} w_{m k_2}^{\ell *}$ . Also we can use the selection rule in the  $3j$  symbols that states that the sum of the bottom row must be equal to zero for the symbol to be non-zero. This gives us

$$M_{k_1 k'_1 k_2 k_3}^{\ell_1 \ell_2} = 64\pi^4 (-1)^{k_2+k_3} \sum_{\ell_4 k_4 k_5} \mathcal{W}_{k_4, k_5}^{\ell_4} \frac{1}{2\ell_4 + 1} \begin{pmatrix} \ell_1 & \ell_2 & \ell_4 \\ k_1 & -k_2 & k_4 \end{pmatrix} \begin{pmatrix} \ell_1 & \ell_2 & \ell_4 \\ k'_1 & -k_3 & k_5 \end{pmatrix} \delta_{k_4, k_2-k_1} \delta_{k_5, k_3-k'_1} \\ = 64\pi^4 (-1)^{k_2+k_3} \sum_{\ell_4} \mathcal{W}_{k_2-k_1, k_3-k'_1}^{\ell_4} \frac{1}{2\ell_4 + 1} \begin{pmatrix} \ell_1 & \ell_2 & \ell_4 \\ k_1 & -k_2 & k_2-k_1 \end{pmatrix} \begin{pmatrix} \ell_1 & \ell_2 & \ell_4 \\ k'_1 & -k_3 & k_3-k'_1 \end{pmatrix}. \quad (\text{B8})$$

### APPENDIX C: SYMMETRIES IN $M_{k_1 k'_1 k_2 k_3}^{\ell_1 \ell_2}$

The symmetries in the matrix  $M_{k_1 k'_1 k_2 k_3}^{\ell_1 \ell_2}$  are important to reduce the computation time. First we look at swapping the indices  $k_2$  and  $k_3$  along with  $k_1$  and  $k'_1$ :

$$M_{k'_1 k_1 k_3 k_2}^{\ell_1 \ell_2} = 64\pi^4 (-1)^{k_2+k_3} \sum_{\ell_4} \mathcal{W}_{k_3-k'_1, k_2-k_1}^{\ell_4} \frac{1}{2\ell_4 + 1} \begin{pmatrix} \ell_1 & \ell_2 & \ell_4 \\ k'_1 & -k_3 & k_3-k'_1 \end{pmatrix} \begin{pmatrix} \ell_1 & \ell_2 & \ell_4 \\ k_1 & -k_2 & k_2-k_1 \end{pmatrix} \\ = 64\pi^4 (-1)^{k_2+k_3} \sum_{\ell_4} \mathcal{W}_{k_2-k_1, k_3-k'_1}^{\ell_4 *} \frac{1}{2\ell_4 + 1} \begin{pmatrix} \ell_1 & \ell_2 & \ell_4 \\ k_1 & -k_2 & k_2-k_1 \end{pmatrix} \begin{pmatrix} \ell_1 & \ell_2 & \ell_4 \\ k_1 & -k_3 & k_3-k'_1 \end{pmatrix} \\ = M_{k_1 k'_1 k_2 k_3}^{\ell_1 \ell_2 *}, \quad (\text{C1})$$

where we have used the definition of window correlation matrix to say that  $\mathcal{W}_{k_2, k_1}^{\ell} = \mathcal{W}_{k_1, k_2}^{\ell *}$ . Now we look at the reversing the sign of all  $k_i$ . This implies that

$$\mathcal{W}_{-k_1, -k_2}^{\ell} = \sum_m w_{m-k_1}^{\ell} w_{m-k_2}^{\ell *} \\ = \sum_m (-1)^{m+k_1} w_{-mk_1}^{\ell *} (-1)^{m+k_1} w_{-mk_2}^{\ell} \\ = (-1)^{k_1+k_2} \mathcal{W}_{k_1, k_2}^{\ell *}. \quad (\text{C2})$$

Now we can show symmetry in the matrix  $M$  is given by

$$\begin{aligned}
M_{-k_1-k'_1-k_2-k_3}^{\ell_1\ell_2} &= 64\pi^2(-1)^{k_2+k_3} \sum_{\ell_4} \mathcal{W}_{-k_2+k_1, -k_3+k'_1}^{\ell_4} \frac{1}{2\ell_4+1} \begin{pmatrix} \ell_1 & \ell_2 & \ell_4 \\ -k_1 & +k_2 & -k_2+k_1 \end{pmatrix} \begin{pmatrix} \ell_1 & \ell_2 & \ell_4 \\ -k'_1 & +k_3 & -k_3+k'_1 \end{pmatrix} \\
&= 64\pi^4(-1)^{k_2+k_3} \sum_{\ell_4} (-1)^{k_2-k_1+k_3-k'_1} \mathcal{W}_{k_2-k_1, k_3-k'_1}^{\ell_4*} \frac{1}{2\ell_4+1} \begin{pmatrix} \ell_1 & \ell_2 & \ell_4 \\ k_1 & -k_2 & k_2-k_1 \end{pmatrix} \begin{pmatrix} \ell_1 & \ell_2 & \ell_4 \\ k'_1 & -k_3 & k_3-k'_1 \end{pmatrix} \\
&= (-1)^{k_2-k_1+k_3-k'_1} M_{k_1k'_1k_2k_3}^{\ell_1\ell_2*},
\end{aligned} \tag{C3}$$

where in the second equality we have used the relation

$$\begin{pmatrix} \ell_1 & \ell_2 & \ell_3 \\ m_1 & m_2 & m_3 \end{pmatrix} \begin{pmatrix} \ell_1 & \ell_2 & \ell_3 \\ m'_1 & m'_2 & m'_3 \end{pmatrix} = \begin{pmatrix} \ell_1 & \ell_2 & \ell_3 \\ -m_1 & -m_2 & -m_3 \end{pmatrix} \begin{pmatrix} \ell_1 & \ell_2 & \ell_3 \\ -m'_1 & -m'_2 & -m'_3 \end{pmatrix}. \tag{C4}$$

#### APPENDIX D: EXPLICIT FORM OF THE COUPLING OPERATOR

In section 3.3 we use the coupling operator  $\mathbf{O}_{i_1 i_2}$ . Here we explicitly write it in terms of the sub operators  $O_{\ell_1 \ell_2}^{k_1 k'_1 s_1 s_2}$

$$\mathbf{O}_{ij} = \begin{pmatrix} O_{\ell_1 \ell_2}^{0000} & O_{\ell_1 \ell_2}^{0002} & O_{\ell_1 \ell_2}^{000-2} & O_{\ell_1 \ell_2}^{0022} & O_{\ell_1 \ell_2}^{002-2} & O_{\ell_1 \ell_2}^{00-2-2} \\ O_{\ell_1 \ell_2}^{0200} & O_{\ell_1 \ell_2}^{0202} & O_{\ell_1 \ell_2}^{020-2} & O_{\ell_1 \ell_2}^{0222} & O_{\ell_1 \ell_2}^{022-2} & O_{\ell_1 \ell_2}^{00-2-2} \\ O_{\ell_1 \ell_2}^{0-200} & O_{\ell_1 \ell_2}^{0-202} & O_{\ell_1 \ell_2}^{0-20-2} & O_{\ell_1 \ell_2}^{0-222} & O_{\ell_1 \ell_2}^{0-22-2} & O_{\ell_1 \ell_2}^{0-2-2-2} \\ O_{\ell_1 \ell_2}^{2200} & O_{\ell_1 \ell_2}^{2202} & O_{\ell_1 \ell_2}^{220-2} & O_{\ell_1 \ell_2}^{2222} & O_{\ell_1 \ell_2}^{222-2} & O_{\ell_1 \ell_2}^{22-2-2} \\ O_{\ell_1 \ell_2}^{2-200} & O_{\ell_1 \ell_2}^{2-202} & O_{\ell_1 \ell_2}^{2-20-2} & O_{\ell_1 \ell_2}^{2-222} & O_{\ell_1 \ell_2}^{2-22-2} & O_{\ell_1 \ell_2}^{2-2-2-2} \\ O_{\ell_1 \ell_2}^{-2-200} & O_{\ell_1 \ell_2}^{-2-202} & O_{\ell_1 \ell_2}^{-2-20-2} & O_{\ell_1 \ell_2}^{-2-222} & O_{\ell_1 \ell_2}^{-2-22-2} & O_{\ell_1 \ell_2}^{-2-2-2-2} \end{pmatrix}.$$

#### APPENDIX E: RELATIONS BETWEEN $C_\ell^{SS'}$ AND $C_\ell^{XY}$

The following matrix operation allows conversion from  $C_\ell^{SS'}$  to  $C_\ell^{XY}$ ,

$$\begin{pmatrix} C_\ell^{TT} \\ C_\ell^{TE} \\ C_\ell^{TB} \\ C_\ell^{EE} \\ C_\ell^{EB} \\ C_\ell^{BB} \end{pmatrix} = \begin{pmatrix} 1 & 0 & 0 & 0 & 0 & 0 \\ 0 & -1/2 & -1/2 & 0 & 0 & 0 \\ 0 & i/2 & -i/2 & 0 & 0 & 0 \\ 0 & 0 & 0 & 1/4 & 1/4 & 1/4 \\ 0 & 0 & 0 & -i/4 & i/4 & -i/4 \\ 0 & 0 & 0 & -1/4 & -1/4 & 1/4 \end{pmatrix} \begin{pmatrix} C_\ell^{00} \\ C_\ell^{02} \\ C_\ell^{0-2} \\ C_\ell^{22} \\ C_\ell^{2-2} \\ C_\ell^{-2-2} \end{pmatrix}. \tag{E1}$$

The matrix is not square, this does not imply that there is more information in the right than the left. There are the same number of degrees of freedom on both sides this is because  $C_\ell^{2-2} = C_\ell^{-22}$ .